Notably, amino acid substitutions at certain sites in NCT ECD differently affected the Aβ generation and Notch processing (20). Thus, search for small compounds or peptides targeting NCT ECD might provide a new class of biological tools as well as therapeutics for γ-secretase modulation. Further investigations including structural analyses of NCT ECD complexed with scFvs would shed light on the molecular mechanism of the functional assembly of γ-secretase and the role of NCT ECD in the γ-secretase-mediated intramembrane cleavage.

Acknowledgments—We acknowledge Drs. Keiro Shirotani (Fukushima Medical University), Harald Steiner, Christian Haass (Ludwig-Maximilians-University), Gopal Thinakaran, Sangram Sisodia (The University of Chicago), Haruhiko Fuwa (Tohoku University), Satoshi Yokoshima, and Tohru Fukuyama (The University of Tokyo) for valuable reagents. We are also grateful to our current/previous laboratory members for helpful discussions and technical assistance.

REFERENCES

1. Tomita, T. (2009) *Expert Rev. Neurother.* **9,** 661–679
2. Wolfe, M. S. (2009) *Semin. Cell Dev. Biol.* **20,** 219–224
3. Takasugi, N., Tomita, T., Hayashi, I., Tsuruoka, M., Niimura, M., Takahashi, Y., Thinakaran, G., and Iwatsubo, T. (2003) *Nature* **422,** 438–441
4. Selkoe, D. J., and Wolfe, M. S. (2007) *Cell* **131,** 215–221
5. Spasic, D., and Annaert, W. (2008) *J. Cell Sci.* **121,** 413–420
6. Sato, C., Morohashi, Y., Tomita, T., and Iwatsubo, T. (2006) *J. Neurosci* **26,** 12081–12088
7. Tolia, A., Chávez-Gutiérrez, L., and De Strooper, B. (2006) *J. Biol. Chem.* **281,** 27633–27642
8. Niimura, M., Isoo, N., Takasugi, N., Tsuruoka, M., Ui-Tei, K., Saigo, K., Morohashi, Y., Tomita, T., and Iwatsubo, T. (2005) *J. Biol. Chem.* **280,** 12967–12975
9. Isoo, N., Sato, C., Miyashita, H., Shinohara, M., Takasugi, N., Morohashi, Y., Tsuji, S., Tomita, T., and Iwatsubo, T. (2007) *J. Biol. Chem.* **282,** 12388–12396
10. Yu, G., Nishimura, M., Arawaka, S., Levitan, D., Zhang, L., Tandon, A., Song, Y. Q., Rogaeva, E., Chen, F., Kawarai, T., Supala, A., Levesque, L., Yu, H., Yang, D. S., Holmes, E., Milman, P., Liang, Y., Zhang, D. M., Xu, D. H., Sato, C., Rogaev, E., Smith, M., Janus, C., Zhang, Y., Aebersold, R., Farrer, L. S., Sorbi, S., Bruni, A., Fraser, P., and St George-Hyslop, P. (2000) *Nature* **407,** 48–54
11. Leem, J. Y., Vijayan, S., Han, P., Cai, D., Machura, M., Lopes, K. O., Veselits, M. L., Xu, H., and Thinakaran, G. (2002) *J. Biol. Chem.* **277,** 19236–19240
12. Kaether, C., Lammich, S., Edbauer, D., Ertl, M., Rietdorf, J., Capell, A., Steiner, H., and Haass, C. (2002) *J. Cell Biol.* **158,** 551–561
13. Kimberly, W. T., LaVoie, M. J., Ostaszewski, B. L., Ye, W., Wolfe, M. S., and Selkoe, D. J. (2002) *J. Biol. Chem.* **277,** 35113–35117
14. Tomita, T., Katayama, R., Takikawa, R., and Iwatsubo, T. (2002) *FEBS Lett.* **520,** 117–121
15. Yang, D. S., Tandon, A., Chen, F., Yu, G., Yu, H., Arawaka, S., Hasegawa, H., Duthie, M., Schmidt, S. D., Ramabhadran, T. V., Nixon, R. A., Mathews, P. M., Gandy, S. E., Mount, H. T., St George-Hyslop, P., and Fraser, P. E. (2002) *J. Biol. Chem.* **277,** 28135–28142
16. Herreman, A., Van Gassen, G., Bentahir, M., Nyabi, O., Craessaerts, K., Mueller, U., Annaert, W., and De Strooper, B. (2003) *J. Cell Sci.* **116,** 1127–1136
17. Shirotani, K., Edbauer, D., Capell, A., Schmitz, J., Steiner, H., and Haass, C. (2003) *J. Biol. Chem.* **278,** 16474–16477
18. Fagan, R., Swindells, M., Overington, J., and Weir, M. (2001) *Trends Biochem. Sci.* **26,** 213–214
19. Shah, S., Lee, S. F., Tabuchi, K., Hao, Y. H., Yu, C., LaPlant, Q., Ball, H., Dann, C. E., 3rd, Südhof, T., and Yu, G. (2005) *Cell* **122,** 435–447
20. Chávez-Gutiérrez, L., Tolia, A., Maes, E., Li, T., Wong, P. C., and de Strooper, B. (2008) *J. Biol. Chem.* **283,** 20096–20105
21. Holliger, P., and Hudson, P. J. (2005) *Nat. Biotechnol.* **23,** 1126–1136
22. Miller, T. W., and Messer, A. (2005) *Mol. Ther.* **12,** 394–401
23. Stocks, M. (2005) *Curr. Opin. Chem. Biol.* **9,** 359–365
24. Verbeke, K., Gils, A., and Declerck, P. J. (2004) *J. Thromb. Haemost.* **2,** 298–305
25. Arbel, M., Yacoby, I., and Solomon, B. (2005) *Proc. Natl. Acad. Sci. U.S.A.* **102,** 7718–7723
26. Gal-Tanamy, M., Zemel, R., Berdichevsky, Y., Bachmatov, L., Tur-Kaspa, R., and Benhar, I. (2005) *J. Mol. Biol.* **347,** 991–1003
27. Paganetti, P., Calanca, V., Galli, C., Stefani, M., and Molinari, M. (2005) *J. Cell Biol.* **168,** 863–868
28. Farady, C. J., Sun, J., Darragh, M. R., Miller, S. M., and Craik, C. S. (2007) *J. Mol. Biol.* **369,** 1041–1051
29. Mikkelsen, J. H., Gyrup, C., Kristensen, P., Overgaard, M. T., Poulsen, C. B., Laursen, L. S., and Oxvig, C. (2008) *J. Biol. Chem.* **283,** 16772–16780
30. Hayashi, I., Urano, Y., Fukuda, R., Isoo, N., Kodama, T., Hamakubo, T., Tomita, T., and Iwatsubo, T. (2004) *J. Biol. Chem.* **279,** 38040–38046
31. Ogura, T., Mio, K., Hayashi, I., Miyashita, H., Fukuda, R., Kopan, R., Kodama, T., Hamakubo, T., Iwatsubo, T., Tomita, T., and Sato, C. (2006) *Biochem. Biophys. Res. Commun.* **343,** 525–534
32. Li, T., Ma, G., Cai, H., Price, D. L., and Wong, P. C. (2003) *J. Neurosci.* **23,** 3272–3277
33. Watanabe, N., Tomita, T., Sato, C., Kitamura, T., Morohashi, Y., and Iwatsubo, T. (2005) *J. Biol. Chem.* **280,** 41967–41975
34. Tomita, T., Takikawa, R., Koyama, A., Morohashi, Y., Takasugi, N., Saido, T. C., Maruyama, K., and Iwatsubo, T. (1999) *J. Neurosci.* **19,** 10627–10634
35. Tomita, T., Watabiki, T., Takikawa, R., Morohashi, Y., Takasugi, N., Kopan, R., De Strooper, B., and Iwatsubo, T. (2001) *J. Biol. Chem.* **276,** 33273–33281
36. Tomita, T., Maruyama, K., Saido, T. C., Kume, H., Shinozaki, K., Tokuhiro, S., Capell, A., Walter, J., Grünberg, J., Haass, C., Iwatsubo, T., and Obata, K. (1997) *Proc. Natl. Acad. Sci. U.S.A.* **94,** 2025–2030
37. Morohashi, Y., Kan, T., Tominari, Y., Fuwa, H., Okamura, Y., Watanabe, N., Sato, C., Natsugari, H., Fukuyama, T., Iwatsubo, T., and Tomita, T. (2006) *J. Biol. Chem.* **281,** 14670–14676
38. Takahashi, Y., Hayashi, I., Tominari, Y., Rikimaru, K., Morohashi, Y., Kan, T., Natsugari, H., Fukuyama, T., Tomita, T., and Iwatsubo, T. (2003) *J. Biol. Chem.* **278,** 18664–18670
39. Fuwa, H., Takahashi, Y., Konno, Y., Watanabe, N., Miyashita, H., Sasaki, M., Natsugari, H., Kan, T., Fukuyama, T., Tomita, T., and Iwatsubo, T. (2007) *ACS Chem. Biol.* **2,** 408–418
40. Saitoh, R., Ohtomo, T., Yamada, Y., Kamada, N., Nezu, J., Kimura, N., Funahashi, S., Furugaki, K., Yoshino, T., Kawase, Y., Kato, A., Ueda, O., Jishage, K., Suzuki, M., Fukuda, R., Arai, M., Iwanari, H., Takahashi, K., Sakihama, T., Ohizumi, I., Kodama, T., Tsuchiya, M., and Hamakubo, T. (2007) *J. Immunol. Methods* **322,** 104–117
41. Walker, E. S., Martinez, M., Wang, J., and Goate, A. (2006) *J. Neurochem.* **98,** 300–309
42. Ratovitski, T., Slunt, H. H., Thinakaran, G., Price, D. L., Sisodia, S. S., and Borchelt, D. R. (1997) *J. Biol. Chem.* **272,** 24536–24541
43. Kato, K., and Kamiya, Y. (2007) *Glycobiology* **17,** 1031–1044
44. Caramelo, J. J., and Parodi, A. J. (2008) *J. Biol. Chem.* **283,** 10221–10225
45. Morais, V. A., Brito, C., Pijak, D. S., Crystal, A. S., Fortna, R. R., Li, T., Wong, P. C., Doms, R. W., and Costa, J. (2006) *Biochim Biophys Acta* **1762,** 802–810
46. Saul, R., Chambers, J. P., Molyneux, R. J., and Elbein, A. D. (1983) *Arch. Biochem. Biophys.* **221,** 593–597
47. Hammond, C., Braakman, I., and Helenius, A. (1994) *Proc. Natl. Acad. Sci. U.S.A.* **91,** 913–917
48. LaVoie, M. J., Fraering, P. C., Ostaszewski, B. L., Ye, W., Kimberly, W. T., Wolfe, M. S., and Selkoe, D. J. (2003) *J. Biol. Chem.* **278,** 37213–37222
49. Capell, A., Beher, D., Prokop, S., Steiner, H., Kaether, C., Shearman, M. S., and Haass, C. (2005) *J. Biol. Chem.* **280,** 6471–6478
50. Kim, S. H., Yin, Y. I., Li, Y. M., and Sisodia, S. S. (2004) *J. Biol. Chem.* **279,** 48615–48619
51. Kaether, C., Scheuermann, J., Fassler, M., Zilow, S., Shirotani, K., Valkova, C., Novak, B., Kacmar, S., Steiner, H., and Haass, C. (2007) *EMBO Rep.* **8,**

743–748
52. Kim, J., Kleizen, B., Choy, R., Thinakaran, G., Sisodia, S. S., and Schekman, R. W. (2007) *J. Cell Biol.* **179,** 951–963
53. Spasic, D., Raemaekers, T., Dillen, K., Declerck, I., Baert, V., Serneels, L., Füllekrug, J., and Annaert, W. (2007) *J. Cell Biol.* **176,** 629–640
54. Keller, S. H., Lindstrom, J., and Taylor, P. (1998) *J. Biol. Chem.* **273,** 17064–17072
55. Marcus, N. Y., and Perlmutter, D. H. (2000) *J. Biol. Chem.* **275,** 1987–1992
56. Sidhu, S. S., and Koide, S. (2007) *Curr. Opin. Struct. Biol.* **17,** 481–487
57. Novoa de Armas, H., Dewilde, M., Verbeke, K., De Maeyer, M., and Declerck, P. J. (2007) *Structure* **15,** 1105–1116

Cancer Science
The official journal of the Japanese Cancer Association JCA

Dual antitumor mechanisms of Notch signaling inhibitor in a T-cell acute lymphoblastic leukemia xenograft model

Shigeo Masuda,[1,2,3] Keiki Kumano,[1,2] Takahiro Suzuki,[1,2] Taisuke Tomita,[4] Takeshi Iwatsubo,[4,5] Hideaki Natsugari,[6] Arinobu Tojo,[7] Makoto Shibutani,[8] Kunitoshi Mitsumori,[8] Yutaka Hanazono,[3] Seishi Ogawa,[1,9] Mineo Kurokawa[2] and Shigeru Chiba[1,10,11]

[1]Department of Cell Therapy and Transplantation Medicine, University of Tokyo Hospital, Tokyo; [2]Department of Hematology and Oncology, Graduate School of Medicine, University of Tokyo, Tokyo; [3]Division of Regenerative Medicine, Center for Molecular Medicine, Jichi Medical University, Tochigi; [4]Department of Neuropathology and Neuroscience, Graduate School of Pharmaceutical Sciences, University of Tokyo, Tokyo; [5]Department of Neuropathology, Graduate School of Medicine, University of Tokyo, Tokyo; [6]Department of Rational Medicinal Science, Graduate School of Pharmaceutical Sciences, University of Tokyo, Tokyo; [7]Department of Hematology and Oncology, Institute of Medical Sciences, University of Tokyo, Tokyo; [8]Laboratory of Veterinary Pathology, Tokyo University of Agriculture and Technology, Tokyo; [9]21th Century COE Program, Graduate School of Medicine, University of Tokyo, Tokyo; [10]Department of Clinical and Experimental Hematology, Graduate School of Comprehensive Human Sciences, University of Tsukuba, Tsukuba, Japan

(Received May 04, 2009/Revised August 19, 2009/Accepted August 21, 2009/Online publication September 23, 2009)

Constitutive activation of Notch signaling is required for the proliferation of a subgroup of human T-cell acute lymphoblastic leukemias (T-ALL). Previous *in vitro* studies have demonstrated the therapeutic potential of Notch signaling inhibitors for treating T-ALL. To further examine this possibility, we applied a γ-secretase inhibitor (GSI) to T-ALL xenograft models. Treatment of established subcutaneous tumors with GSI resulted in partial or complete regression of tumors arising from four T-ALL cell lines that were also sensitive to GSI *in vitro*. To elucidate the mechanism of action, we transduced DND-41 cells with the active form of Notch1 (aN1), which conferred resistance to *in vitro* GSI treatment. Nevertheless, *in vivo* treatment with GSI induced a partial but significant regression of subcutaneous tumors that developed from aN1-transduced DND-41 cells, whereas it induced complete regression of tumors that developed from mock-transduced DND-41 cells. These findings indicate that the remarkable efficacy of GSI might be attributable to dual mechanisms, directly via apoptosis of DND-41 cells through the inhibition of cell-autonomous Notch signaling, and indirectly via disturbance of tumor angiogenesis through the inhibition of non-cell-autonomous Notch signaling. (*Cancer Sci* 2009; 100: 2444–2450)

The Notch signaling pathway has a crucial role in a variety of cellular functions, including cell proliferation, differentiation, and apoptosis.[1,2] Notch proteins are heterodimeric transmembrane receptors composed of an extracellular subunit and a transmembrane subunit, and associate with each other via heterodimerization (HD) domains in the extracellular regions. Notch signaling, initiated by receptor-ligand interactions, requires subsequent proteolytic cleavage of the receptor by several proteases, resulting in liberation of the cleaved form of Notch1 that is functionally active (hereafter referred to as aN1) as it translocates into the nucleus and up-regulates the transcription of Notch-RBP-Jκ-regulated genes.[3]

Recent studies in tumorigenesis of hematologic malignancies and solid tumors have revealed several examples of aberrant Notch signaling.[2,4,5] Forced expression of aN1 in mouse bone marrow results in the development of T-cell leukemia,[6] and more importantly, amplified Notch signaling contributes to approximately 50% of human T-cell acute lymphoblastic leukemia (T-ALL).[7,8] The Notch signal amplification in T-ALL is due to gain-of-function mutations in the *NOTCH1* gene, which have also been detected in many different murine T-ALL models.[9–12] *NOTCH1* activating mutations cluster at the HD and intracellular domains, leading to ligand-independent cleavage and activation of Notch1, and increased stability of aN1, respectively. Notch1 signaling, whether initiated by receptor–ligand interactions or triggered by *NOTCH1*-activating mutations in the HD domains, eventually depends on the proteolytic activity of γ-secretase. γ-Secretase inhibitors (GSIs), available as small molecular compounds, suppress Notch signaling by blocking the activity of the γ-secretase complex.[13] Previous studies have demonstrated that blockade of Notch signaling with GSI induces cell cycle arrest and apoptosis in a subset of human T-ALL cell lines,[7,14,15] and an early phase clinical trial has already been conducted.[16] Despite that, precise mechanisms of action of GSI on T-ALL *in vivo* are yet to be elucidated.

Here, to examine the potential clinical applications for GSIs in T-ALL patients, and to evaluate the mechanisms of GSI action, we investigated the effects of the GSI compound YO01027[17] (referred to hereafter as YO) on human T-ALL growth in murine xenograft models, because YO administration to mice induced defective melanocyte stem cell maintenance but kept the mice otherwise healthy as shown in our previous paper.[18] The results here indicated that YO is highly effective against T-ALL growth *in vivo* and demonstrated that the efficacy of GSI might be due to the inhibition of Notch signaling via two mechanisms.

Materials and Methods

Cell cultures and reagents. Human T-ALL cell lines (ALL-SIL, DND-41, HPB-ALL, KOPT-K1, TALL-1, MOLT-4, PF-382, and CEM) were obtained from the Fujisaki Cell Center, Hayashibara Biochemical Laboratories (Okayama, Japan), maintained in RPMI supplemented with 10% fetal bovine serum and penicillin/streptomycin, and incubated at 37°C with 5% CO_2. Human umbilical vein endothelial cells (HUVEC; Lonza Walkersville, Walkersville, MD, USA) were cultured in Endothelial Basal Medium-2 (Lonza Walkersville) and SingleQuots (Lonza Walkersville). The YO, which is an LY-411,575 analogue, was synthesized as described previously.[17] YO was dissolved in dimethyl sulfoxide (DMSO) to create 10 mM or 50 mM stock solutions.

Animals. SCID mice (C.B-17/Icr-*scid*/*scid*Jcl; 6 weeks old, female) were purchased from CLEA Japan (Tokyo, Japan) and

[11]To whom correspondence should be addressed. E-mail: schiba-tky@umin.net

doi: 10.1111/j.1349-7006.2009.01328.x

maintained under specific pathogen-free conditions. All experimental procedures were performed in accordance with the guidelines for animal experiments of the University of Tokyo and Jichi Medical University.

Xenograft mouse model. SCID mice at 6–8 weeks of age were inoculated subcutaneously in the right flank with 3×10^7 cells in 300 μL of phosphate buffered saline. In concurrent administration experiments, the mice were assigned to a control group and a YO-treated group the day after tumor inoculation. YO was orally administered daily for at least 30 days at a dose of 0.1 or 1 mg/kg/day. In challenge experiments for established tumors, mice were similarly assigned as described above at approximately 2.5–3 weeks (in HPB-ALL and TALL-1) or 8–12 weeks (in ALL-SIL and DND-41) after tumor cell inoculation, when tumor size had reached a certain volume. YO was orally administered daily at a dose of 0.1, 1, or 10 mg/kg/day. Tumor size was measured at the greatest length and width. The volume was calculated as $1/2 \times (\text{tumor length}) \times (\text{tumor width})^2$.

***In vivo* administration of YO.** *In vivo* administration of YO was performed as described previously.[19] Briefly, 0.1–10 mg/kg of YO or an equal volume of vehicle (DMSO) in 300 μL of 0.5% methylcellulose (Wako, Osaka, Japan) was administered orally to SCID mice using a disposable oral zonde (Fuchigami, Kyoto, Japan) once a day for the indicated periods.

Plasmid construction and retroviral transduction. The cDNA for myc-tagged murine aN1[20] was subcloned into the *Bam*HI restriction site of the retrovirus vector pMYs/internal ribosomal entry site-enhanced green fluorescent protein (IRES-EGFP; pMYs/IG).[21] Retroviral transduction of a human T-ALL cell line, DND-41, was performed using PLAT-F cells as described previously.[21] Following transduction, GFP-positive cells were sorted to 90% purity and used for further analysis. The proteins were detected by Western blotting using an anti-myc antibody (9E10).

Proliferation assay. Cell growth was quantified using a WST-1-based assay (Cell Counting Kit-8; Dojindo Medical Technologies, Kumamoto, Japan), which is a highly sensitive colorimetric assay. Briefly, human T-ALL cell lines (3×10^4 cells/well) or HUVEC (4×10^3 cells/well) were seeded into 96-well plates. Vascular endothelial growth factor (VEGF; 100 ng/mL) was supplemented in the medium for HUVEC. Various concentrations of YO were added, and proliferation was measured in duplicate at 7 days or 11 days using a WST-1-based assay according to the manufacturer's instructions. Proliferation was expressed as a percentage or fold change of vehicle-treated controls. Results are expressed as mean value ± SD.

Detection of apoptosis. Cells were incubated with various concentrations of YO for the indicated periods. Apoptosis was assessed using a fluorescein isothiocyanate-labeled Annexin V staining kit (Immunotech; Beckman-Coulter, Prague, Czech Republic) combined with 7-amino-actinomycin D (7-AAD), according to the manufacturer's instructions, with a FACS Calibur cytometer (BD Biosciences, San Jose, CA, USA).

TUNEL staining. To detect apoptotic cells, ALL-SIL-bearing SCID mice were sacrificed after the treatment with 1 mg/kg YO or vehicle for 5 days. Frozen blocks of tumors were cryosectioned and fixed with 1% paraformaldehyde, followed by analysis for apoptosis using the ApopTag Plus Peroxidase *In Situ* Apoptosis Detection Kit (Millipore, Billerica, MA, USA) according to the manufacturer's instructions.

Western blotting. Western blotting was performed as described previously.[22] The probes used were antibodies against cleaved Notch1 (Val1744; Cell Signaling Technology, Danvers, MA, USA) and GAPDH as a control. The Val1744 antibody was incubated at a dilution of 1:1000 overnight.

Tube formation assay. Upon the BD BioCoat Angiogenesis Plate (96 well), 2×10^4 HUVEC were seeded per well, with or without 100 nM YO. After 18 h, cells were stained with fluores-

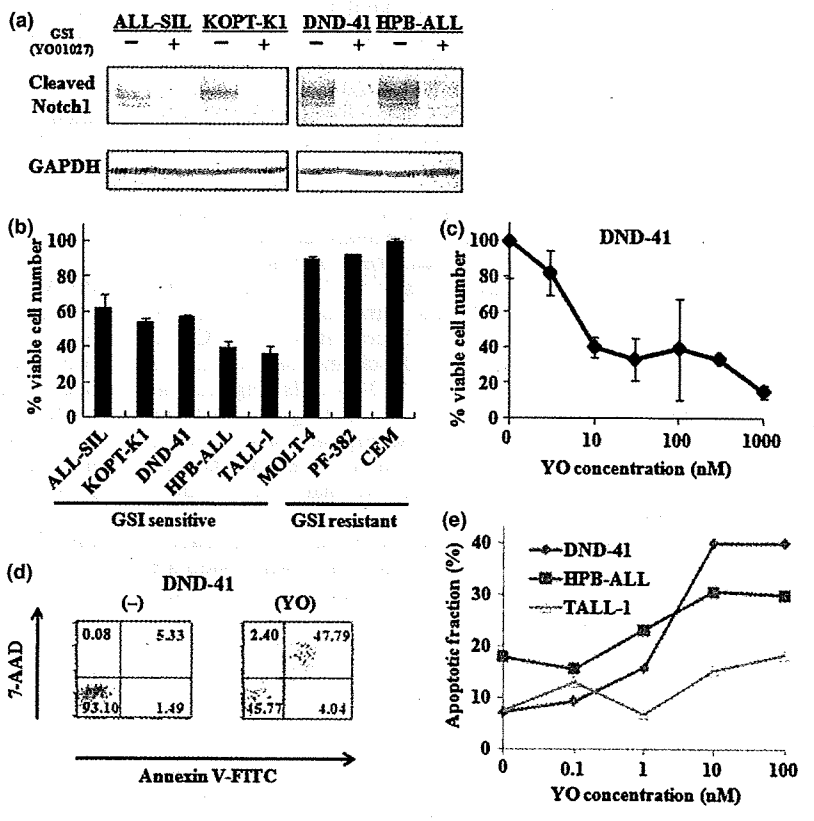

Fig. 1. Inhibition of Notch signaling impairs growth of human T-cell acute lymphoblastic leukemias (T-ALL) cell lines. (a) Western blot analysis for cleaved Notch1 in human T-ALL cell lines treated with 100 nM YO01027 for 48 h. GAPDH is shown as a loading control. (b) Proliferation assay of a panel of human T-ALL cell lines treated for 7 days with 100 nM YO01027 or vehicle control. The percent of viable cell number indicates the proportion of viable cells in the treated populations relative to untreated populations. (c) Dose dependent effects of YO01027 on the proliferation of DND-41 cell line treated for 7 days with 3, 10, 30, 100, 300, 1000 nM YO01027 or vehicle control. The percent of viable cell number indicates the proportion of viable cells in the treated populations relative to untreated populations. (d) Annexin V assay of DND-41 cell line treated for 7 days with 10 nM YO01027 or vehicle control. (e) Dose dependent effects of YO01027 on the apoptosis of human T-ALL cell lines treated for 7 days with 0.1, 1, 10, 100 nM YO01027 or vehicle control. The apoptotic fraction denotes the fraction of Annexin V (+)/7-AAD (+) cells, and the percent of apoptotic fraction indicates the proportion of apoptotic cells among the total cells within each treated well.

cent dye, Calcein AM (BD Biosciences), according to the manufacturer's instructions. Images were captured with the BIOREVO BZ-9000 microscope (Keyence, Osaka, Japan), and the tube length was measured using the BZ-H1C image analysis application (Keyence).

Histological analysis. Frozen blocks were cryosectioned at 5 μm and mounted on slides. Histological sections were air-dried and fixed in acetone for 15 min, followed by immunostaining with a 1:200 dilution of antimouse CD31 antibody (clone; MEC13.3) (BD-Pharmingen, San Diego, CA, USA) overnight at 4°C. Horseradish peroxide with the coloring agent diaminobenzidine was used as the substrate. Sections were then counterstained with hematoxylin. Vessel counting was performed at ×40 magnification in several randomly chosen areas.

Statistics. Statistical analyses were performed using the Student's *t*-test. A *P*-value of <0.05 was considered statistically significant.

Results

Human T-ALL lines are susceptible to Notch inhibition. Some human T-ALL cell lines with *NOTCH1* activating mutations are sensitive to GSI *in vitro*.[7,13–15] We examined the ability of YO, a GSI compound that has not been tested in cell-based experiments, to inhibit Notch signaling. Various human T-ALL cell lines (ALL-SIL, KOPT-K1, DND-41, and HPB-ALL) were treated with YO for 48 h followed by immunoblotting with cleaved Notch1 (Val1744) antibody, which can specifically detect the aN1 proteins. Treatment of these cell lines with 100 nM YO resulted in an almost complete block of Notch1 activity (Fig. 1a).

To investigate the anti-proliferative effect of YO on T-ALL cells, we measured cellular viability using the WST-1-based assay in human T-ALL cell lines after YO treatment. As expected, YO exerted an anti-proliferative effect on some T-ALL cell lines (ALL-SIL, KOPT-K1, HPB-ALL, DND-41, and TALL-1), whereas other cell lines (MOLT-4, PF-382, and CEM) were not sensitive to this compound (Fig. 1b). To examine concentration dependency, DND-41 was treated with various concentrations of YO for 7 days and applied to the WST-1-based assay. A steep concentration dependency was observed between 1 nM and 10 nM. The effect was virtually saturated at >10 nM (Fig. 1c).

Next, we explored whether the decreased proliferation of T-ALL cell lines after treatment with YO was due to the induction of cell cycle arrest and/or apoptosis. We analyzed the cell cycle of the T-ALL cell lines after YO treatment using flow cytometry. As expected from previous reports,[7,13–15] YO induced G0-G1 arrest in all the T-ALL cell lines sensitive to YO (data not shown). Then, we treated five T-ALL cell lines with YO for 7 days followed by Annexin V/7-AAD staining, and found that YO induced significant apoptosis of DND-41 cells (Fig. 1d), as well as the other T-ALL cell lines tested (Fig. 1e). Similar results were observed using a pharmacologically distinct GSI, DAPT, known to block Notch activation (data not shown). Taken together, these results confirmed that some human T-ALL cell lines are susceptible to YO treatment *in vitro*.

Concurrent administration of YO with tumor inoculation results in the inhibition of tumor growth in T-ALL xenograft models. To examine *in vivo* antitumor effects of YO, we used murine xenograft models, in which SCID mice were inoculated subcutaneously with human cell lines. HPB-ALL and TALL-1 cell lines established subcutaneous tumors 2.5–3 weeks after inoculation. The subcutaneous tumors of the YO-treated groups were significantly smaller than those of control groups 2.5–4 weeks after the inoculation and the initiation of concurrent administration of YO or vehicle. Notably, in mice treated with 1 mg/kg of YO, there was no tumor formation observed in any of the TALL-1-inoculated mice or in approximately half the HPB-ALL-inoculated mice (Fig. 2a,b). This result indicates that YO exerts *in vivo* antitumor effects on T-ALL, at least during the period of tumor engraftment.

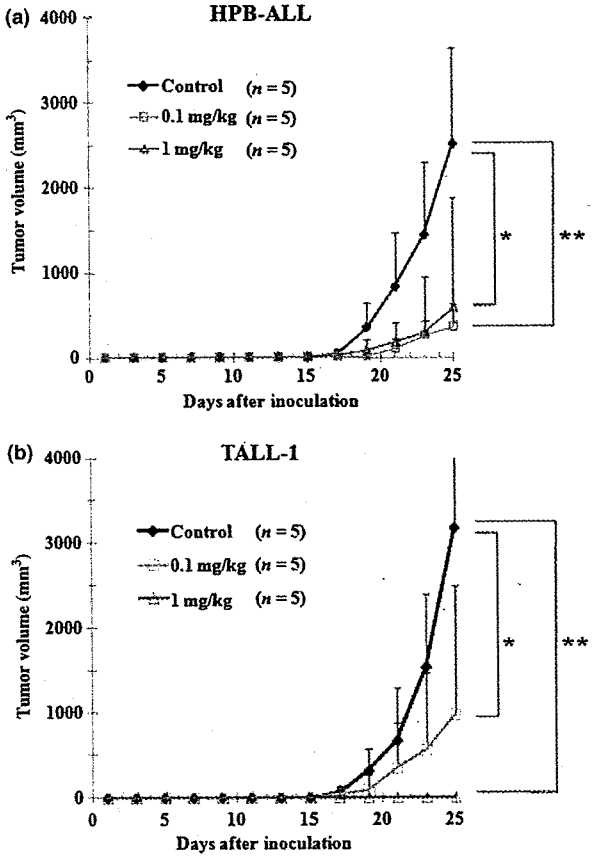

Fig. 2. Antitumor effects of YO01027 (YO) on xenograft models of human T-cell acute lymphoblastic leukemias (T-ALL), with concurrent administration of YO with tumor inoculation. Mice were inoculated subcutaneously with HPB-ALL (a) or TALL-1 cell lines (b). The next day, mice were randomly assigned to receive vehicle alone or varying doses of YO01027 daily, as described in "Materials and Methods". Data represent the mean tumor volume (mm^3) ±SD grown in vehicle-treated mice, YO (0.1 mg/kg)-treated mice, or YO (1 mg/kg)-treated mice. *$P < 0.05$; **$P < 0.01$, statistically significant differences (vehicle *vs* YO).

YO treatment against established tumors in T-ALL xenograft models results in partial or complete regression. Next, we evaluated the effects of YO treatment when the tumors grew to visible sizes. In this experimental design, YO treatment resulted in partial (HPB-ALL) or complete (ALL-SIL, DND-41, and TALL-1) regression of the established subcutaneous tumors. When treated with 10 mg/kg/day YO, the growth of tumors derived from HPB-ALL was suppressed to <50% compared with growth without treatment. Tumors derived from ALL-SIL, DND-41, and TALL-1 completely regressed within 2–3 weeks following treatment with YO at 1 mg/kg/day (Fig. 3a).

To confirm the *in vivo* pharmacologic inhibition of Notch signaling by YO, we excised tumors made of ALL-SIL from mice with or without 1 or 10 mg/kg/day YO treatment for 3 days, followed by immunoblotting of the tumor lysates with the Val1744 antibody. The level of cleaved Notch1 was reduced partially or almost completely after 1 or 10 mg/kg/day YO treatment, respectively. Thus, YO administered at both

doi: 10.1111/j.1349-7006.2009.01328.x

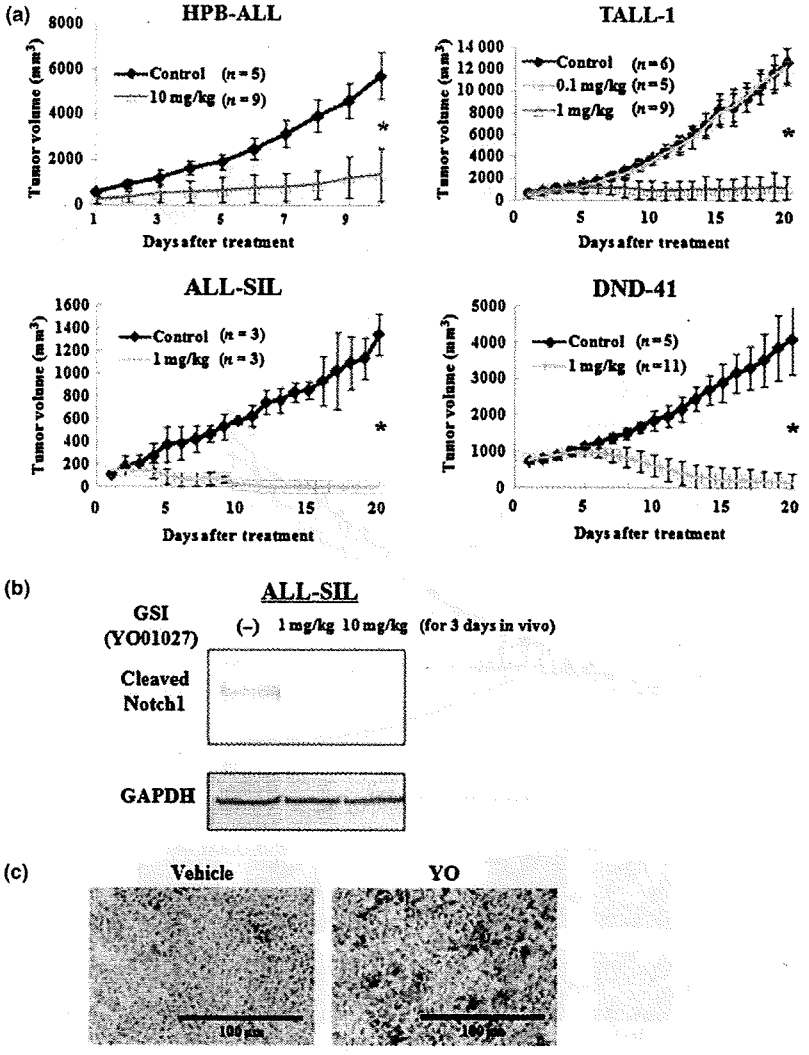

Fig. 3. Antitumor effects of YO01027 (YO) on xenograft models of human T-cell acute lymphoblastic leukemias (T-ALL), with YO treatment after tumor establishment. (a) Mice were inoculated subcutaneously with HPB-ALL, TALL-1, DND-41, or ALL-SIL cell lines. When the diameter of the tumor reached 12–13 mm, mice were randomly assigned to receive vehicle alone or varying doses of YO01027 daily, as described in the "Materials and Methods". Data represent the mean tumor volume (mm^3) ±SD grown in vehicle-treated mice or YO (0.1 or 1 or 10 mg/kg)-treated mice. *$P < 0.001$, statistically significant differences (vehicle *vs* YO). (b) Western blot analysis for cleaved Notch1 in engrafted tumors treated with YO. ALL-SIL-challenged mice were treated daily with vehicle alone or YO, and tumors were harvested 72 h after the initiation of treatment, followed by Western blotting of tumor lysates with cleaved Notch1 (Val1744) antibody. GAPDH is shown as a loading control. (c) YO treatment induces apoptosis of ALL-SIL cells *in vivo*. ALL-SIL-bearing mice were treated daily with vehicle alone or YO01027 at a dose of 1 mg/kg, and tumors were harvested 5 days after the initiation of treatment. Tumor sections were fixed with 1% paraformaldehyde and apoptotic cells were stained using TUNEL assay.

1 mg/kg/day and 10 mg/kg/day to SCID mice was pharmacologically active, and blocked Notch1 signaling partially or almost completely, at least in cells of subcutaneous tumors (Fig. 3b).

To determine whether YO treatment induces apoptosis *in vivo*, we performed TUNEL staining on tumors made of ALL-SIL, which was isolated from vehicle- or YO-treated mice. TUNEL-positive cells were reproducibly increased in number by the YO treatment (Fig. 3c), demonstrating increased apoptosis of T-ALL cells *in vivo*.

Effect of aN1 expression in tumor growth during YO treatment. We next expressed aN1 exogenously in DND-41 cell lines to examine whether aN1 rescues YO-induced cell growth arrest and tumor regression. aN1 represents a protein that is already cleaved, and is thus not a substrate for γ-secretase. Therefore, it was expected that DND-41 cells transduced with aN1 (hereafter referred to as DND-41/aN1) would become resistant to YO treatment.

We established DND-41/aN1 cells by infection of parental DNA-41 cells with aN1-expressing retrovirus, followed by bulk sorting of GFP-positive cells. Expression of aN1 proteins was confirmed by Western blotting with an anti-myc antibody (Fig. 4a). Parental DND-41 and mock-infected DND-41 (DND-41/mock) were sensitive to YO, but, as expected, DND-41/aN1 was substantially resistant to YO *in vitro* when assessed by a cell proliferation assay (Fig. 4b). The continuous presence of 100 nM YO allowed for selection of cells highly resistant to YO (DND-41/aN1/GSI; Fig. 4b). The *in vitro* growth curves of these cells under basal conditions (without YO) were very similar to each other (data not shown).

We implanted parental DND-41, DND-41/mock, DND-41/aN1, and DND-41/aN1/GSI cells subcutaneously into SCID mice. Subcutaneous tumors began to be palpable and the tumor volume reached 700 mm^3 in 8–12 weeks. Treatment with YO at 1 mg/kg/day or control vehicle was then initiated. In vehicle-treated mice, the tumors derived from parental DND-41, DND-41/mock, DND-41/aN1, and DND-41/aN1/GSI cells grew in a similar manner, whereas YO treatment resulted in a substantial regression of the tumors derived from parental DND-41 and DND-41/mock cells (Fig. 4c,d). Interestingly, *in vivo* YO treatment of tumors derived from DND-41/aN1 and DND-41/aN1/GSI cells, which were resistant to YO *in vitro*, induced significantly slower cell growth compared with the vehicle treatment, suggesting that these cells were sensitive to YO to some degree *in vivo* (Fig. 4c,d). In some mice, we observed a stabilization of the tumor volume. Nevertheless, YO treatment was not sufficiently effective on DND-41/aN1 and DND-41/aN1/GSI to regress the tumors to an impalpable level, unlike parental DND-41- and DND-41/mock-derived tumors.

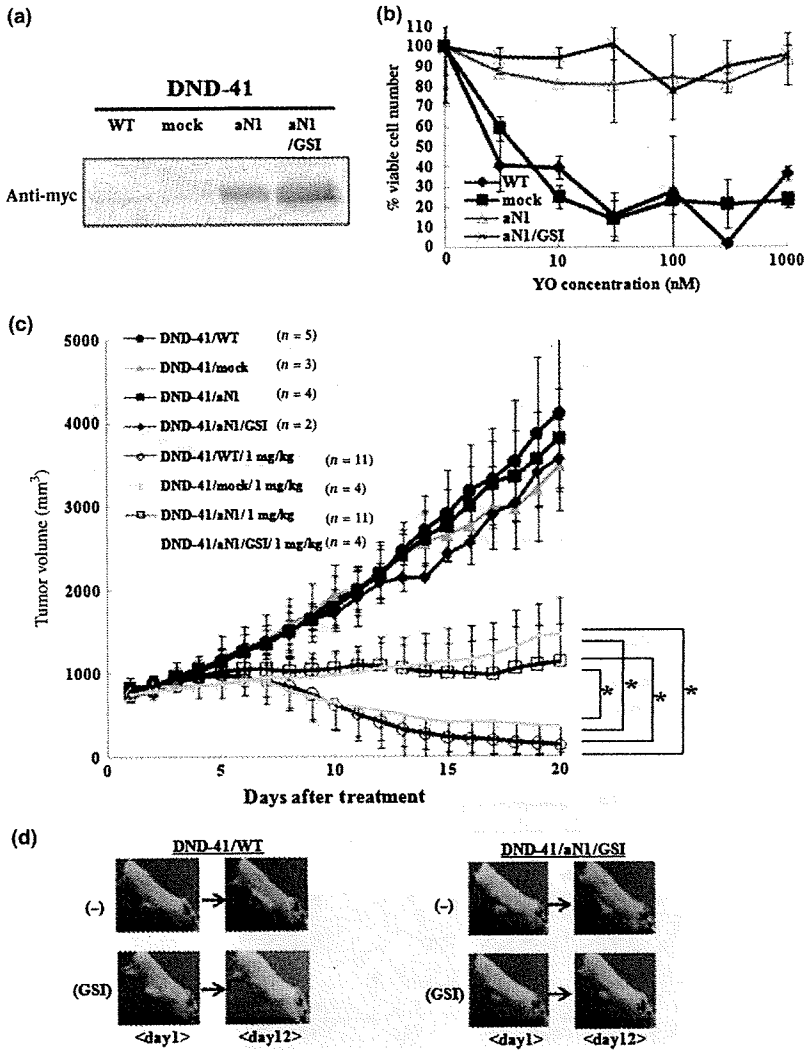

Fig. 4. Establishment of DND-41/aN1 and effects of aN1 rescue on tumor growth during YO01027 (YO) treatment. (a) Expression of aN1 proteins tagged with myc in DND-41/aN1 cells and DND-41/aN1/GSI cells was confirmed by Western blotting analysis. (b) Proliferation assay of established DND-41/aN1 and DND-41/aN1/GSI cell lines, compared with DND-41/WT and DND-41/mock cell lines, after treatment for 11 days with varying doses of YO. The percent of viable cell number indicates the proportion of viable cells in the treated populations relative to untreated populations. (c) Antitumor effects of YO on xenograft models of DND-41/WT, DND-41/mock, DND-41/aN1, and DND-41/aN1/GSI (pre-selected by γ-secretase inhibitor [GSI] *in vitro*). "1 mg/kg/day" denotes the group that received the YO treatment at a dose of 1 mg/kg/day. Data represent the mean tumor volume (mm^3) ±SD of vehicle-treated mice or YO (1 mg/kg)-treated mice. *$P < 0.01$, statistically significant differences. (d) Representative appearance of subcutaneous xenograft models during YO treatment. DND-41 cells stably expressing control vector or aN1 (pre-selected by GSI *in vitro*) were grown as xenografts in SCID mice. Representative mice from each group are shown.

Effect of YO on *in vitro* tube formation and *in vivo* tumor vessels. Recent studies have demonstrated that inhibition of Notch signaling in solid tumors resulted in tumor regression via increased tumor vessels with poor perfusion.[23–26] It has been shown that Notch inhibition leads to promotion of non-functioning angiogenesis.

Tube formation assay was performed to investigate the effect of YO on *in vitro* angiogenesis using HUVEC. We found that YO treatment significantly increased the tube length in the tube formation assay (Fig. 5a,b), suggesting that Notch inhibition promoted proliferation of endothelial cells, which is consistent with previous studies.[24,27] In addition, cell proliferation in the presence of VEGF was measured with WST-1-based assay. YO significantly promoted proliferation of HUVEC (Fig. 5c) as previously reported.[24,27]

To further clarify the mechanism of action with YO treatment, we analyzed the tumor vasculature during YO treatment. We implanted DND-41 cells into SCID mice and started YO or vehicle treatment after the tumor diameter reached approximately 1 cm. We sacrificed mice at treatment day 5, and analyzed tumor sections by immunostaining for anti-CD31, which is able to identify the vessels in tumors. In the average, approximately 30 and >40 vessels per mm^2 were observed in the vehicle-treated and YO-treated mice, respectively (Fig. 5d,e). These results are consistent with the previous reports described above, in which tumor regression would result from increased but poorly functional tumor vessels. Collectively, tumor regression in our models may depend partially on the disrupted tumor vasculature with paradoxically increased tumor vessels presumably through the inhibition of non-cell-autonomous Notch signaling by YO.

Discussion

The findings of the present study confirmed that the YO compound that we synthesized is a GSI that efficiently blocks Notch signaling in T-ALL cell lines carrying activating *NOTCH1* mutations and induces apoptosis of these cell lines *in vitro*. The cell-autonomous effect against Notch signaling described here is postulated to be the mechanism of anti-T-ALL, creating the bases for clinical studies of a GSI targeting T-ALL.

We demonstrated a marked *in vivo* effect of YO in a xenograft model that was more dramatic than we had expected. Although the mechanisms of YO action on T-ALL have been virtually confined to the cell-autonomous Notch signal inhibition, including a recent report describing the combinatorial effect of steroid with GSI,[28] the strong effect of GSI *in vivo* could also be attributed to non-cell-autonomous inhibition of Notch signaling.

Our findings were consistent with the recent reports on the role of Notch signaling in tumor angiogenesis.[23–26] Delta-4, one of the Notch ligands, is expressed on tip cells in the endothe-

doi: 10.1111/j.1349-7006.2009.01328.x

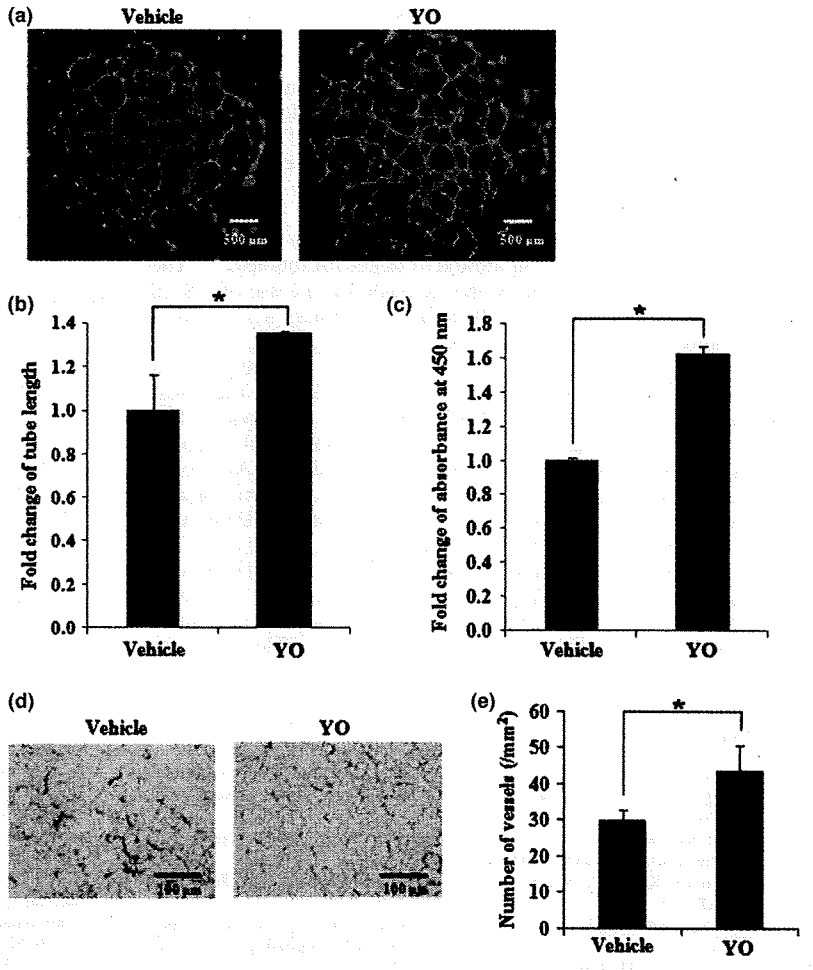

Fig. 5. *In vitro* and *in vivo* analysis of vascular cells after YO01027 (YO) treatment. (a) The *in vitro* tube formation analysis of HUVEC, either with or without 100 nM YO treatment. The cells were stained with fluorescent dye, Calcein AM, and the representative images are shown. Original magnification, ×20. (b) Quantitative analysis of tube length after tube formation of HUVEC with or without 100 nM YO. Fold change of tube length is shown, compared with that of vehicle control. $*P < 0.05$, statistically significant differences. (c) The cell proliferation assay of HUVEC in the presence of vascular endothelial growth factor (VEGF), either with or without 100 nM YO for 7 days. Fold change of absorbance at 450 nm is shown, compared with that of the vehicle control. $*P < 0.05$, statistically significant differences. (d) Anti-CD31 immunostainings of tumor sections in DND-41-bearing SCID mice, either after YO treatment at a dose of 1 mg/kg/day or after vehicle treatment. Original magnification, ×40. (e) Quantitative analysis of vessels in tumors after YO treatment. The cells stained with anti-CD31 were counted, and data represent the mean vessel density (per mm^2) ±SD in tumors derived from DND-41. $*P < 0.05$, statistically significant differences.

lium of newly elongating tumor vessels by stimulation with VEGF. Engagement of Notch1 expressed on the stalk cells in the endothelium by neighboring tip cell-expressing Delta-4 blocks differentiation of the stalk cells into tip cells, which represents the process required for the normally functioning tumor vessel formation. Blockade of this signaling pathway impairs normal tumor angiogenesis and creates hyper-blanched, non-functioning vasculature, which results in regression of the solid tumor. Whereas we used T-ALL cell lines in our experiments, we chose the subcutaneous tumor injection model because it is more convenient for observing and measuring the tumors. In this subcutaneous tumor model, we observed a similar tendency regarding tumor vessel density, from which we could easily speculate that the same mechanism was underlying this phenomenon.

The introduction of the GSI-insensitive cleaved form of Notch1 into DND-41 cells transformed these cells to be completely resistant to YO *in vitro*, exactly as expected, but failed to confer complete resistance to YO in the subcutaneous xenograft model. Whereas the subcutaneous tumors derived from DND-41/aN1 were significantly more resistant to YO than tumors derived from parental DND-41 and DND-41/mock cells, they still significantly responded to YO. These observations fit the idea that the marked *in vivo* antitumor effect of YO against subcutaneous tumors derived from parental DND-41 as well as DND-41/mock cells was mediated through, in addition to the cell-autonomous effect, a blockade of tumor vasculature that supplies blood to the tumor cells in a non-cell-autonomous fashion.

We confirmed that subcutaneous tumors made of a colon cancer cell line, LoVo, which was non-sensitive to YO *in vitro*, were partially regressed by YO at 10 mg/kg/day (data not shown). The effect of YO on the LoVo tumors, however, was not as strong as on tumors made of parental DND-41 and several other T-ALL cell lines, again supporting the idea that the exceptionally strong effect of YO on T-ALL xenografts is due to the inhibiting effect of YO on Notch signaling at two independent targets *in vivo*.

As shown in Figure 3(b), inhibition of Notch1 activation *in vivo* was almost complete with YO at 10 mg/kg but incomplete with YO at 1 mg/kg. On the other hand, the effect of YO *in vitro* was saturated by YO >10 nM, as shown in Figure 1(c). These findings might indicate that >10 nM serum/tissue concentration is achieved with 10 mg/kg and 1–10 nM with 1 mg/kg administration, if both *in vitro* and *in vivo* results are considered together. Whereas administration of YO at 1–3 mg/kg/day for up to 4 weeks did not cause weight loss, diarrhea, or hair coat abnormalities in mice, treatment at 10 mg/kg/day for more than 2 weeks resulted in obvious weight loss, diarrhea, and hair coat roughness. This implies a narrow window of YO for the treatment purpose. Nevertheless, it also indicates that the sensitivity to YO is variable among tissues and cells, and this difference might be important for YO to be considered as a drug. Together with the results described in previous papers,[18,29,30] a subset of T-ALL cells may be the most sensitive among others and possibly similar to melenocyte stem cells and splenic marginal zone B cells. In contrast, thymocyte progenitors and intestinal goblet cells appear to be less sensitive to YO.

Based on the facts that subcutaneous tumors from T-ALL cell lines do not represent common clinical presentations and that

our finding might depend on the experimental model that we chose in this study, the question arises as to how the current findings can be translated to clinical application. The vasculature component might be negligible in the leukemia model, but the effect of the combination of cell-autonomous apoptosis induction in leukemia cells with the inhibition of angiogenesis in leukemic cell-infiltrating bone marrow is not known. The effectiveness of YO in a leukemia model must be examined using the same T-ALL cell lines.

The discovery of *NOTCH1* activating mutations in T-ALL has made the Notch pathway an attractive target for therapy.[31] The results described here indicate the rationale for the use of GSI in the treatment of T-ALL, as well as for solid tumors whose tumor vasculature formation is dependent on Notch signaling.

Nevertheless, resistance of T-ALL against GSI might limit the clinical use of GSI. Recently, mutational loss of the phosphatase and tensin homolog (PTEN) gene, which encodes a key tumor suppressor that inhibits the phosphatidylinositol-3 kinase (PI3K)–Akt signaling pathway, was discovered in T-ALL cells that are resistant to GSI.[32] This could explain the variation of GSI sensitivity among T-ALL cells. Our results with HPB-ALL raise a different issue. This cell line was very sensitive to YO *in vitro*, but subcutaneous tumors derived from HPB-ALL appeared to be less sensitive to YO compared to other cells such as DND-41. This result indicates that YO concentrations sufficient to inhibit Notch1 activation may not be achieved in the subcutaneous tumor made from HPB-ALL. In addition, it is likely that inhibition of tumor vessel formation is less efficient for the reduction of subcutaneous HPB-ALL tumors for some reasons, such that this particular tumor is less dependent on tumor vessels.

Expectations and questions are intermingled with regard to the development of GSI and other Notch signal inhibitors for the treatment of T-ALL as well as other tumors. Nevertheless, various Notch signal inhibitors are being developed aiming at clinical use.

Acknowledgments

We thank Toshio Kitamura (Institute of Medical Science, University of Tokyo) for the pMYs/IRES-EGFP retrovirus vector and Akira Harashima (Hayashibara Biomedical Laboratories) for the T-ALL cell lines (ALL-SIL, DND-41, HPB-ALL, KOPT-K1, TALL-1, MOLT-4, PF-382, and CEM). This work was supported in part by Grants-in-Aid for Scientific Research (KAKENHI nos. 17014023, 18013012, and 19390258) from the Ministry of Education, Culture, Sports, Science and Technology (MEXT) of Japan, and a Research Grant from the Sagawa Foundation of Promotion of Cancer Sciences to S.C.; Grants-in-Aid for Young Scientists (KAKENHI nos. 17790637 and 19790660) from MEXT; research funding for young scientists from the Science and Technology Foundation of Japan; research funding from the Japan Leukemia Research Fund; and research funding from Aichi Cancer Research Foundation to S.M.

References

1 Grabher C, von Boehmer H, Look AT. Notch 1 activation in the molecular pathogenesis of T-cell acute lymphoblastic leukaemia. *Nat Rev Cancer* 2006; **6**: 347–59.
2 Leong KG, Karsan A. Recent insights into the role of Notch signaling in tumorigenesis. *Blood* 2006; **107**: 2223–33.
3 Mumm JS, Kopan R. Notch signaling: from the outside in. *Dev Biol* 2000; **228**: 151–65.
4 Pear WS, Aster JC. T cell acute lymphoblastic leukemia/lymphoma: a human cancer commonly associated with aberrant NOTCH1 signaling. *Curr Opin Hematol* 2004; **11**: 426–33.
5 Lee SY, Kumano K, Nakazaki K *et al.* Gain-of-function mutations and copy number increases of Notch2 in diffuse large B-cell lymphoma. *Cancer Sci* 2009; **100**: 920–6.
6 Pear WS, Aster JC, Scott ML *et al.* Exclusive development of T cell neoplasms in mice transplanted with bone marrow expressing activated Notch alleles. *J Exp Med* 1996; **183**: 2283–91.
7 Weng AP, Ferrando AA, Lee W *et al.* Activating mutations of NOTCH1 in human T cell acute lymphoblastic leukemia. *Science* 2004; **306**: 269–71.
8 Lee SY, Kumano K, Masuda S *et al.* Mutations of the Notch1 gene in T-cell acute lymphoblastic leukemia: analysis in adults and children. *Leukemia* 2005; **19**: 1841–3.
9 Dumortier A, Jeannet R, Kirstetter P *et al.* Notch activation is an early and critical event during T-Cell leukemogenesis in Ikaros-deficient mice. *Mol Cell Biol* 2006; **26**: 209–20.
10 Lin YW, Nichols RA, Letterio JJ, Aplan PD. Notch1 mutations are important for leukemic transformation in murine models of precursor-T leukemia/lymphoma. *Blood* 2006; **107**: 2540–3.
11 O'Neil J, Calvo J, McKenna K *et al.* Activating Notch1 mutations in mouse models of T-ALL. *Blood* 2006; **107**: 781–5.
12 Reschly EJ, Spaulding C, Vilimas T *et al.* Notch1 promotes survival of E2A-deficient T cell lymphomas through pre-T cell receptor-dependent and -independent mechanisms. *Blood* 2006; **107**: 4115–21.
13 Weng AP, Nam Y, Wolfe MS *et al.* Growth suppression of pre-T acute lymphoblastic leukemia cells by inhibition of notch signaling. *Mol Cell Biol* 2003; **23**: 655–64.
14 Lewis HD, Leveridge M, Strack PR *et al.* Apoptosis in T cell acute lymphoblastic leukemia cells after cell cycle arrest induced by pharmacological inhibition of Notch signaling. *Chem Biol* 2007; **14**: 209–19.
15 O'Neil J, Grim J, Strack P *et al.* FBW7 mutations in leukemic cells mediate NOTCH pathway activation and resistance to γ-secretase inhibitors. *J Exp Med* 2007; **204**: 1813–24.
16 Shih IeM, Wang TL. Notch signaling, γ-secretase inhibitors, and cancer therapy. *Cancer Res* 2007; **67**: 1879–82.
17 Fuwa H, Okamura Y, Morohashi Y *et al.* Highly efficient synthesis of medium-sized lactams via intramolecular Staudingeraza-Wittig reaction of w-azido pentafluorophenyl ester: synthesis and biological evaluation of Ly411575 analogues. *Tetrahedron Lett* 2004; **45**: 2323–6.
18 Kumano K, Masuda S, Sata M *et al.* Both Notch1 and Notch2 contribute to the regulation of melanocyte homeostasis. *Pigment Cell Melanoma Res* 2008; **21**: 70–8.
19 Wong GT, Manfra D, Poulet FM *et al.* Chronic treatment with the gamma-secretase inhibitor LY-411,575 inhibits beta-amyloid peptide production and alters lymphopoiesis and intestinal cell differentiation. *J Biol Chem* 2004; **279**: 12876–82.
20 Kumano K, Chiba S, Kunisato A *et al.* Notch1 but not Notch2 is essential for generating hematopoietic stem cells from endothelial cells. *Immunity* 2003; **18**: 699–711.
21 Kitamura T, Koshino Y, Shibata F *et al.* Retrovirus-mediated gene transfer and expression cloning: powerful tools in functional genomics. *Exp Hematol* 2003; **31**: 1007–14.
22 Masuda S, Kumano K, Shimizu K *et al.* Notch1 oncoprotein antagonizes TGF-beta/Smad-mediated cell growth suppression via sequestration of coactivator p300. *Cancer Sci* 2005; **96**: 274–82.
23 Noguera-Troise I, Daly C, Papadopoulos NJ *et al.* Blockade of Dll4 inhibits tumour growth by promoting non-productive angiogenesis. *Nature* 2006; **444**: 1032–7.
24 Ridgway J, Zhang G, Wu Y *et al.* Inhibition of Dll4 signalling inhibits tumour growth by deregulating angiogenesis. *Nature* 2006; **444**: 1083–7.
25 Hellstrom M, Phng LK, Hofmann JJ *et al.* Dll4 signalling through Notch1 regulates formation of tip cells during angiogenesis. *Nature* 2007; **445**: 776–80.
26 Siekmann AF, Lawson ND. Notch signalling limits angiogenic cell behaviour in developing zebrafish arteries. *Nature* 2007; **445**: 781–4.
27 Yamanda S, Ebihara S, Asada M *et al.* Role of ephrinB2 in nonproductive angiogenesis induced by Delta-like 4 blockade. *Blood* 2009; **113**: 3631–9.
28 Real PJ, Tosello V, Palomero T *et al.* Gamma-secretase inhibitors reverse glucocorticoid resistance in T cell acute lymphoblastic leukemia. *Nat Med* 2009; **15**: 50–8.
29 Radtke F, Wilson A, Stark G *et al.* Deficient T cell fate specification in mice with an induced inactivation of Notch1. *Immunity* 1999; **10**: 547–58.
30 Saito T, Chiba S, Ichikawa M *et al.* Notch2 is preferentially expressed in mature B cells and indispensable for marginal zone B lineage development. *Immunity* 2003; **18**: 675–85.
31 Aster JC. Deregulated NOTCH signaling in acute T-cell lymphoblastic leukemia/lymphoma: new insights, questions, and opportunities. *Int J Hematol* 2005; **82**: 295–301.
32 Palomero T, Sulis ML, Cortina M *et al.* Mutational loss of PTEN induces resistance to NOTCH1 inhibition in T-cell leukemia. *Nat Med* 2007; **13**: 1203–10.

doi: 10.1111/j.1349-7006.2009.01328.x

BRAIN RESEARCH 1250 (2009) 232–241

available at www.sciencedirect.com

ScienceDirect

www.elsevier.com/locate/brainres

BRAIN RESEARCH

Research Report

Motor impairment and aberrant production of neurochemicals in human α-synuclein A30P+A53T transgenic mice with α-synuclein pathology☆

Masaki Ikeda[a], *Takeshi Kawarabayashi*[b], *Yasuo Harigaya*[d], *Atsushi Sasaki*[c], *Shuichi Yamada*[g], *Etsuro Matsubara*[e], *Tetsuro Murakami*[f], *Yuya Tanaka*[f], *Tomoko Kurata*[f], *Xu Wuhua*[f], *Kenji Ueda*[h], *Hisashi Kuribara*[i], *Yasushi Ikarashi*[j], *Yoichi Nakazato*[c], *Koichi Okamoto*[a], *Koji Abe*[f], *Mikio Shoji*[b,*]

[a]*Department of Neurology, Gunma University Graduate School of Medicine, Maebashi, Japan*
[b]*Department of Neurology, Hirosaki University School of Medicine, Hirosaki, Japan*
[c]*Department of Human Pathology, Gunma University Graduate School of Medicine, Maebashi, Japan*
[d]*Department of Neurology, Maebashi Red Cross Hospital, Maebashi, Gunma, Japan*
[e]*Department of Alzheimer's Disease Research, National Institute for Longevity Sciences, Obu, Japan*
[f]*Department of Neurology, Neuroscience, Biophysiological Science, Okayama University Graduate School of Medicine and Dentistry, Okayama, Japan*
[g]*Immuno-Biological Laboratories Co., Ltd., Mikasa, Hokkaidio, Japan*
[h]*Department of Neural Plasticity, Tokyo Institute of Psychiatry, Setagaya-ku, Tokyo, Japan*
[i]*Tokyo University of Social Welfare, Isesaki, Japan*
[j]*R and D Division, Tsumura and Co., Ltd, Inashiki, Japan*

ARTICLE INFO

Article history:
Accepted 6 October 2008
Available online 1 November 2008

Keywords:
α-synuclein
Mutation
Transgenic mouse
Parkinson's disease
Neurochemical

ABSTRACT

Missense point mutations, duplication and triplication in the α-synuclein (αSYN) gene have been identified in familial Parkinson's disease (PD). Familial and sporadic PD show common pathological features of αSYN pathologies, e.g., Lewy bodies (LBs) and Lewy neurites (LNs), and a loss of dopaminergic neurons in the substantia nigra that leads to motor disturbances. To elucidate the mechanism of αSYN pathologies, we generated TgαSYN transgenic mice overexpressing human αSYN with double mutations in A30P and A53T. Human αSYN accumulated widely in neurons, processes and aberrant neuronal inclusion bodies. Sarcosyl-insoluble αSYN, as well as phosphorylated, ubiquitinated and nitrated αSYN, was accumulated in the brains. Significantly decreased levels of dopamine (DA) were recognized in the striatum. Motor impairment was revealed in a rotarod test. Thus, TgαSYN is a useful model for analyzing the pathological cascade from aggregated αSYN to motor disturbance, and may be useful for drug trials.

☆ Grant numbers and sources of supports: Supported by **Grant-in-Aid for** Grants-in-Aid for Primary Amyloidosis Research Committee (M. S.), from the Ministry of Health, Labor and Welfare of Japan and by Grants-in-Aid for Scientific Research (B) (M.S.: 19390233, K.A.: 18390257), (C) (M.I.: 19590980, T.K.: 19590976, A.S.: 18500276, E.M.: 18590968), from the Ministry of Education, Culture, Sports, Science and Technology, Japan.

* *Corresponding author.* Fax: +81 172 39 5143.
E-mail address: mshoji@hirosaki-u.ac.jp (M. Shoji).

0006-8993/$ – see front matter © 2008 Published by Elsevier B.V.
doi:10.1016/j.brainres.2008.10.011

1. Introduction

αSYN was originally isolated from senile plaques in Alzheimer's disease as a protein of 35 highly hydrophobic amino acid metabolites, known as the non-amyloid component (NAC), derived from a 140 amino-acid precursor encoded by a gene on chromosome 4 (Ueda et al., 1992; Chen et al., 1995), which has homology to rat and Torpedo αSYN and songbird synelfin (George et al., 1995). αSYN is highly abundant in presynaptic terminals (Iwai et al., 1995) and has potential roles in synaptic function and neural plasticity (George et al., 1995; Clayton and George, 1998).αSYN binds to phospholipid vesicles and inhibits PLD2, a regulator of vesicle membrane budding (Liscovitch et al., 2000; Lotharius and Brundin, 2000; Payton et al., 2000), and also plays modulatory roles in the release of dopamine vesicles (Abeliovich et al., 2000).

A few cases of familial Parkinson's disease (FPD) have been linked to missense point mutations in αSYN with A53T (Polymeropoulos et al., 1997), A30P (Kruger et al., 1998) and E46K (PARK1) (Zarranz et al., 2004). Soon after the first A53T missense mutation of αSYN was discovered, the main component of Lewy bodies (LBs) was identified as insoluble aggregates of αSYN (Baba et al., 1998). αSYN and phosphorylated-Ser129 αSYN accumulated in LBs and Lewy neurites (LNs) in PD and Dementia with Lewy bodies (DLB) (Fujiwara et al., 2002; Hasegawa et al., 2002). Then, a second causative gene known as *parkin* (Kitada et al., 1998) was found in familial autosomal recessive juvenile Parkinson's disease (PARK2). *Parkin* ubiquitinates αSYN normally and this process is aberrantly altered in PD (Shimura et al., 2001). Acceleration of oligomerization or protofibrillization is a common property of mutant αSYN (Conway et al., 2001; Choi et al., 2004). Recently, triplication of the αSYN locus (PARK4) was identified in an "Iowanian kindred" with autosomal dominant Lewy body disease (Singleton et al., 2002). Subsequently, duplication of the αSYN gene locus was also reported as a cause of familial PD (Chartier-Harlin et al., 2004). These findings suggest that overexpression of wild type αSYN also leads to facilitation of insoluble aggregation of αSYN. α-synucleinopathy is a disease entity which shares common pathological accumulation of insoluble aggregates of αSYN in the neurons and processes of PD, DLB, Hallervorden–Spatz disease, pure autonomic failure and in the glial cells of multiple system atrophy (MSA) (Goedert, 2000; Hardy and Gwinn-Hardy, 1998; Spillantini et al., 1997; Tu et al., 1998; Galvin et al., 2000; Shoji et al., 2000; Arai et al., 2000).

To elucidate the pathological mechanism of LBs and LNs associated with the decrease in dopamine (DA) production, it is necessary to investigate the aberrant mechanism of mutant αSYN, which is an essential molecule consisting of LBs and LNs (Baba et al., 1998). Here, we generated transgenic (Tg) mice expressing human mutant αSYN A30P+A53T under a human Thy-1 promoter, named as TgαSYN. Overexpression of double mutant human αSYN was expected to lead to further synergistic effects and induce severe α-synucleinopathies and neurodegeneration (Citron et al., 1998; Chishti et al., 2001). TgαSYN showed significant motor impairment in rotarod test, accumulation of insoluble αSYN, aberrant inclusions and decreased dopamine levels. These findings indicate that TgαSYN is a useful animal model to investigate the crucial pathogenesis of α-synucleinopathies, and it may help to develop therapeutic agents.

2. Results

2.1. *Expression of αSYN in transgenic mice and analyses of RT-PCR*

We used the transgene construct hThy1-αSYN A30P+A53T to generate transgenic (Tg) mice, TgαSYN (Fig. 1a). PCR analysis of tail-derived DNA revealed 18 positive Tg mice for human αSYN and EGFP among 129 F0 mice. Five of the 18 Tg mice showed the strongest green fluorescence under irradiation at 365 nm ultraviolet (Fig. 1b). These selected independent lines (#8707, #8713, #8718, #8812, #8819) were mated with BDF1 mice and raised for examination. The following Tg mice were analyzed: 18 positive Tg progenies, 60 F1 Tg (#8707: 2, #8713: 31, #8718: 5, #8812: 10, #8819: 12) and 135 F2 Tg (#8707: 0, #8713: 101, #8718: 2, #8812: 29, #8819: 3). The mRNA expressions of human αSYN A30P+A53T and EGFP in TgαSYN brains were confirmed by RT-PCR, showing the same expression levels of human αSYN A30P+A53T and EGFP at three, eight and 17 months old, respectively (Figs. 1c and d). Western blot using LB509 recognized a 16 kD band corresponding to human αSYN only in Tg mice. AB5038 recognized a 16 kD band corresponding to both human and mouse αSYN. The expression level of human αSYN was 130% of that of endogenous mouse αSYN (Fig. 1e).

2.2. *Histological studies*

Immunocytochemistry of sagittal sections of a seven-month-old #8707 TgαSYN brain by LB509 revealed extensive human αSYN immunostaining in the brainstem, hippocampus, thalamus, cerebral cortex and cerebellum (Fig. 2a, arrow indicates the substantia nigra), but no staining in the non-Tg mouse (Fig. 2b). The TgαSYN brain showed atrophy of the cerebral cortex and cerebellum (Fig. 2a). The HE stain showed eosinophilic inclusion bodies and vacuoles in the cytoplasm of neurons in the substantia nigra (Fig. 2c, arrow), and in the dentate nucleus of TgαSYN (Fig. 2h, arrow). These cytoplasmic inclusions were stained with human-αSYN specific antibody, LB509 (Fig. 2d, arrow, and Fig. 2i, arrow), and anti-αSYN antibody, 42/α-Synuclein (Fig. 2j, arrows). Nitrated α/β synuclein was also stained in the cytoplasmic inclusions (Fig. 2e, arrow,). Ubiquitin-positive inclusions were observed in neurons at brainstem (Fig. 2f, arrow), and dystrophic neurites in the dentate nucleus of TgαSYN (Fig. 2g). Staining of phosphorylated synuclein showed diffuse staining in somatodendrites of TgαSYN neurons (Fig. 2k). Gallyas–Braak staining revealed dystrophic neurites in the dentate nucleus of TgαSYN (Fig. 2l) in ubiquitin-positive structures in the same region (Fig. 2g). Anti-tyrosine hydroxylase (TH) immuno-positive neurons in the locus ceruleus showed weak immunostaining intensity in TgαSYN (Fig. 2m), compared with those of non-Tg mice brains (Fig. 2n). The intensity of substance P immunopositive synapses in the striata of TgαSYN brains (Fig. 2o) was weaker than that of non-Tg mice brains (Fig. 2p). Severe astrocytosis

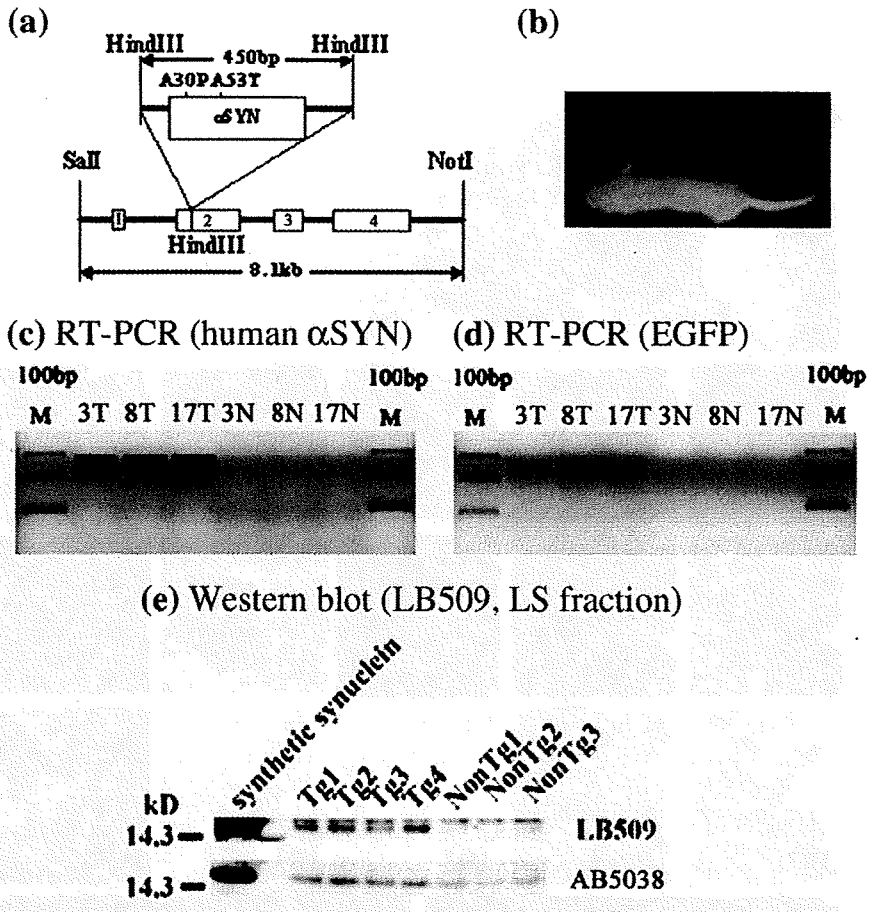

Fig. 1 – The mutant αSYN A30P+A53T construct and the expression of EGFP. (a) The structure of the construct: hThy1-αSYN A30P+A53T. (b) TgαSYN (#8713) showed fluorescence by EGFP (enhanced green fluorescence protein) under 365 nm long wave UV (EGFP-negative non-Tg mouse in the upper location, EGFP-positive Tg mouse in the lower location). (c) Analyses of RT-PCR transcripts: Human αSYN mRNA transcripts (exons 2–4) were detected as 280 bp in TgαSYN brains, but not in non-Tg mice brains, and the intensity of PCR products was the same level as three-, eight-, and 17-month-old Tg mice brains. (d) EGFP mRNA transcripts were detected in TgαSYN brains at the same level at three, eight and 17 months of age, but not in non-Tg mice brains (N showed non-Tg mice brains, T showed Tg mice brains). (e) The expression of human αSYN was detected as a 16 kD band at the same size as recombinant synthetic αSYN by Western blot using LB509 in LS-soluble fractions of TgαSYN #8713 (Tg1–4) mice brains, but not in three 14-month-old non-Tg mice brains (upper lane). AB5038 recognized a 16 kD band corresponding to human and mouse αSYN (lower lane). The expression level of human αSYN was about 130% of that of endogenous mouse αSYN. Synthetic αSYN (SS) was used as a marker of 16 kD αSYN (BIOMOL Research Laboratories Inc., Plymouth Meeting, PA).

was observed in the cerebellum of a 16-month-old TgαSYN (Fig. 2q). An EM study demonstrated cytoplasmic inclusions (Fig. 2r, arrow) and intranuclear inclusions (Fig. 2s, arrows) in the neurons of the brainstem. These inclusion bodies lacked the typical halo and fibrillar structure of LBs.

2.3. *Western blot analysis*

Fourteen-month-old TgαSYN showed a 16 kD band corresponding to αSYN in the LS-soluble fraction (L), Triton-soluble fraction (T), sarcosyl-soluble (S) and sarcosyl-insoluble fractions (I) (Fig. 3a: arrow). In sarcosyl-insoluble fraction, smear pattern was detected in TgαSYN#8812(T3), which accumulated much synuclein histologically. The anti-phosphorylated αSYN antibody pSyn#64 labeled the same size band as αSYN, 16 kD (Fig. 3b: arrow). These findings presented that sarcosyl-insoluble human αSYN and phosphorylated αSYN was accumulated in TgαSYN brains as reported in DLB brains (Hasegawa et al., 2002).

2.4. *Rotarod test for motor function of TgαSYN*

The rotarod test demonstrated that significant motor impairment appeared after a shorter time in TgαSYN; they dropped from the rotating rod faster than non-Tg littermates. The motor impairment was found at three months of age ($p<0.01$) and thereafter deteriorated with age ($p<0.001$. Fig. 4).

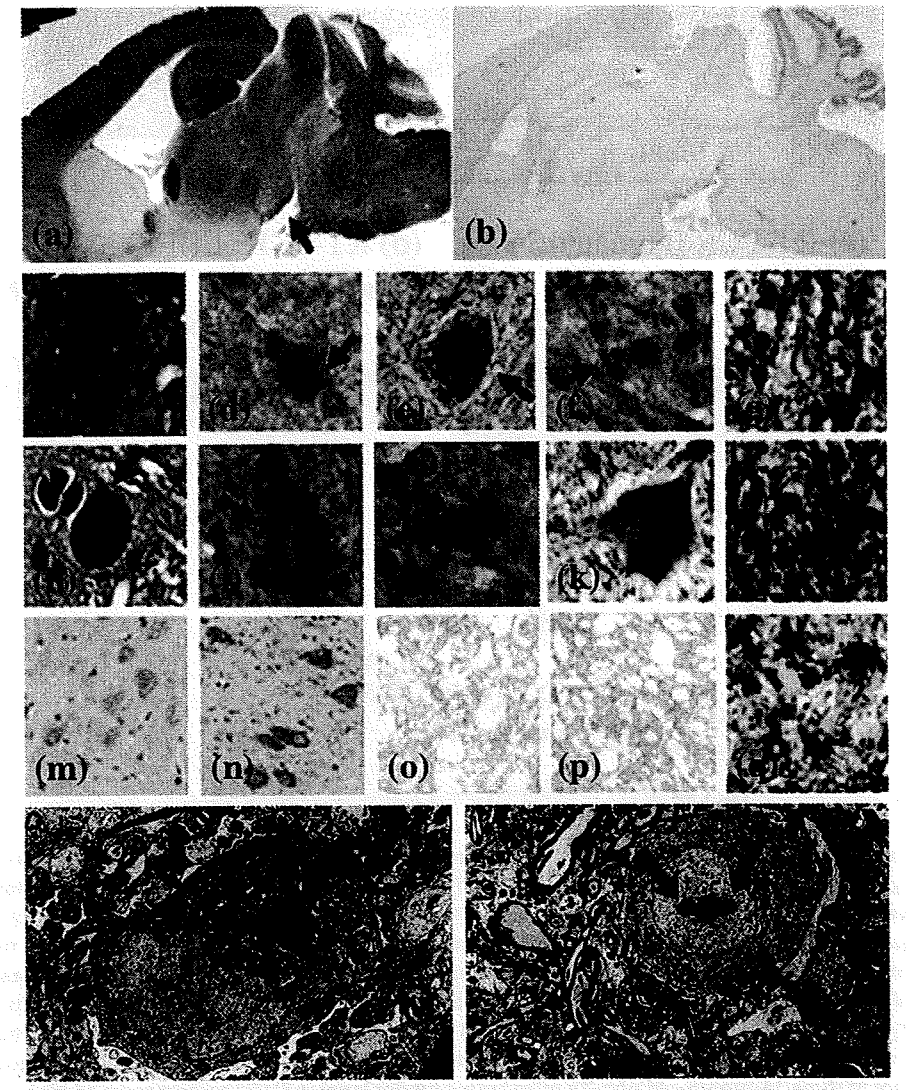

Fig. 2–The pathological features of TgαSYN at seven months of age and age-matched non-Tg mice. (a) A sagittal section of a seven-month-old #8707 TgαSYN brain labeled by LB509 showed extensive αSYN accumulation prominently in the brainstem, hippocampus, thalamus, cerebellum and cerebral cortex. The substantia nigra of the midbrain is also labeled (arrow). The cerebral cortex and cerebellum showed atrophy. (b) No staining in the non-Tg mice brain by LB509. (c) Hematoxylin–eosin stain showed eosinophilic inclusion bodies and vacuoles in the cytoplasm of neurons in the substantia nigra of #8707 TgαSYN (arrow). (d) LB509 detected cytoplasmic inclusions in the substantia nigra of #8707 TgαSYN (arrow). (e) Anti-nitrated α/β SYN monoclonal antibody (Syn12) immunostained cytoplasmic inclusions in the substantia nigra (arrow), as well as in 14-month-old #8713 TgαSYN. (f) Ubiquitin-positive inclusions are shown in the substantia nigra of #8707 TgαSYN (arrow). (g) Ubiquitin-positive dystrophic neurites in the cerebellum dentate of 16-month-old #8713 TgαSYN. (h) Eosinophilic cytoplasmic inclusions (arrow) in the dentate nucleus of #8707 TgαSYN. (i) LB509-positive inclusion in the dentate nucleus of #8707 TgαSYN (arrow). (j) Cytoplasmic inclusions immunostained with a mouse monoclonal antibody 42/α-Synuclein in the brainstem of #8812 TgαSYN (arrow). (k) The PSer129 αSYN antibody immunostained the cytoplasm of neurons in the substantia nigra of #8707 TgαSYN. (l) Gallyas–Braak stain of dystrophic neurites in the dentate nucleus of a 16-month-old #8713 TgαSYN. (m) Tyrosine hydroxylase (TH) immuno-positive neurons in the locus ceruleus showed less immunostaining in the #8707 TgαSYN brain, than the non-Tg mouse brain (n). (o) The intensity of substance P immuno-positive synapses in the striatum of #8707 TgαSYN brain was lower than non-Tg mice brain (p). (q) Astrocytosis in the cerebellum of 16-month-old #8713 TgαSYN. (r) Electron-dense inclusions were found in the cytoplasm of neurons in the brainstems of 8-month-old #8718 TgαSYN by an EM study (arrow). (s) In the brainstem of the same mouse, intracellular inclusions (arrows) were also detected. Scale bar=1 mm in a, b, 12.5 μm in c–f, h–k, 50 μm in g, l, m, n, 25 μm in o, p, and 0.38 μm in r, s.

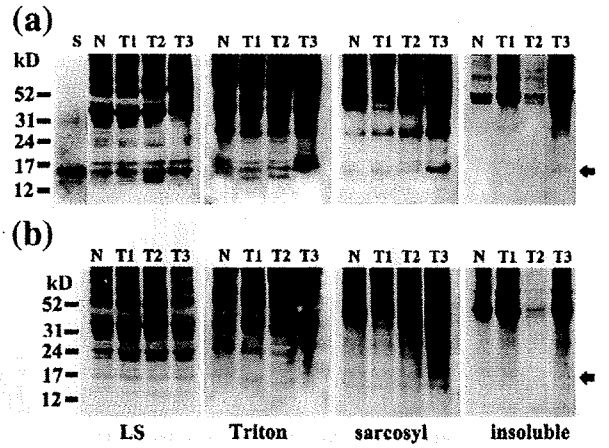

Fig. 3 – Western blot analysis. The expression of human αSYN was 16 kD (lane S; corresponded to recombinant human αSYN) by Western blot using antibody LB509 (a) and pSyn#64 (b) in LS-soluble (L), Triton-soluble (T), sarcosyl-soluble (S) and sarcosyl-insoluble (I) fractions of non-Tg (N), TgαSYN#8713 (T1), TgαSYN#8819 (T2), and TgαSYN#8812 (T3), 14-month-old mice brains.

2.5. *Measurement of neurochemicals*

There was no significant difference in brain weight among Tg and non-Tg mice at 10 and 17 months of age. Compared with age-matched non-Tg control mice, the levels of DA in the striatum were significantly decreased in 10 month-old (p=0.0159) and 17 month-old mice brains (p=0.0286). DA decreased approximately 17% to 24% in the striatum of TgαSYN brains (Fig. 5a). A significant decrease in DA was also detected in the hypothalamuses of 17-month-old TgαSYN brains (p=0.0079. Fig. 5b). NE was not decreased in any areas of 10-month-old TgαSYN brains (Fig. 5c). Serotonin was decreased in the hypothalamuses of 10- and 17-month-old TgαSYN brains (p=0.0079, p=0.0286, respectively. Fig. 5d). ACh decreased in the striatum in 17-month-old TgαSYN (p=0.0286. Fig. 5e). There was no significant alteration in DOPAC, HVA, MHPG, 5-HIAA and Ch levels in any areas of TgαSYN (data not shown). These results showed that insoluble mutant αSYN aggregation selectively decreased the DA level at 10 and 17 months of age.

3. Discussion

Several groups have already reported animal models of PD, such as wild-type αSYN Tg mice (Masliah et al., 2000), mutant αSYN Tg mice (van der Putten et al., 2000, Kahle et al., 2000, Giasson et al., 2002, Lee et al., 2002, Richfield et al., 2002, Neumann et al., 2002, Thiruchelvam et al., 2004, Tofaris et al. 2006, Wakamatsu et al., 2008), *Drosophila melanogaster* (Pendleton et al., 2002) and *C. elegans* (Kuwahara et al., 2006). The first αSYN Tg mice expressed wild-type human αSYN driven by the PDGF-β promoter (Masliah et al., 2000). This mouse displayed intraneuronal inclusions immunoreactive for αSYN and ubiquitin in several regions typically affected in α-synucleinopathies, while lacking the characteristic fibrillar components of Lewy bodies. The Tg mice overexpressing αSYN A53T developed under the murine Thy-1 regulatory sequence showed an early and dramatic decline in motor function (van der Putten et al., 2000). Transgenic wild-type and A30P αSYN abnormally accumulated in neuronal cell bodies and neurites throughout the brain (Kahle et al., 2000). Mice expressing wild-type or A53T αSYN under the mouse prion promoter developed motor deficits by eight months of age (Giasson et al., 2002). Neuropathological assessment of these Tg mice revealed a wide distribution of αSYN, with a pathological sparing of the motor cortex and a total sparing of the substantia nigra. Another group developed Tg mice harboring αSYN A53T using a mouse prion promoter showing motor dysfunction and αSYN accumulation (Lee et al., 2002). Truncated human αSYN (C-120) Tg mice under the TH promoter led to pathological changes in dopaminergic nerve cells of the substantia nigra and olfactory bulb (Tofaris et al., 2006). Recently, truncated human αSYN (C-130) Tg mice also led to selective loss of dopaminergic neurons and accumulation of phosphorylated αSYN (Wakamatsu et al., 2007, 2008).

One of the differences between these models and our TgαSYN was a novel combination of a promoter and mutation of αSYN. TgαSYN expressed double mutant αSYN with A30P +A53T under the human Thy-1 promoter. As expected, our TgαSYN demonstrated widespread αSYN accumulation in the brainstem, caudate putamen, cerebellum, hippocampus and cerebral cortex. Eosinophilic inclusion bodies in the substantia nigra and dentate nucleus of the cerebellum corresponded to accumulation of αSYN. Accumulated αSYN was ubiquitinated, nitrated and phosphorylated at the histological levels as shown in PD and DLB brain. Unfortunately, these inclusion bodies were not compatible with typical LBs because of the absence of a halo structure. At the EM level, fibrillar structure was not observed in inclusion bodies, but they were composed of massive aberrant fine granular structures. Aberrant inclusion bodies with modified αSYN were also observed widely. Since Gallyas–Braak staining labeled these LNs, accumulated αSYN in these neurites may have characteristics of those in β-sheet pleated structures.

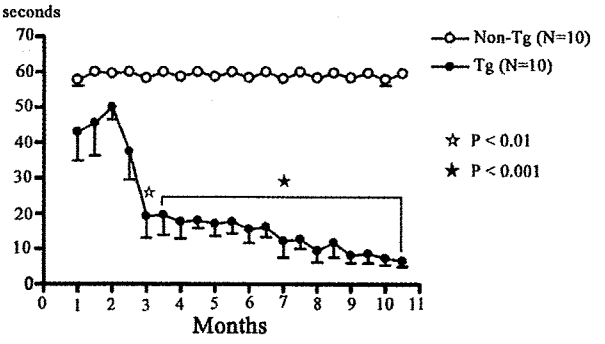

Fig. 4 – Rotarod test. The retention time of Tg mice on the rotarod significantly decreased in TgαSYN. The significant difference began to decrease at three months old (☆: p<0.01) and progressively deteriorated in an age-dependent manner from six months (★: p<0.001). Statistics were analyzed by two-way repeated measures ANOVA.

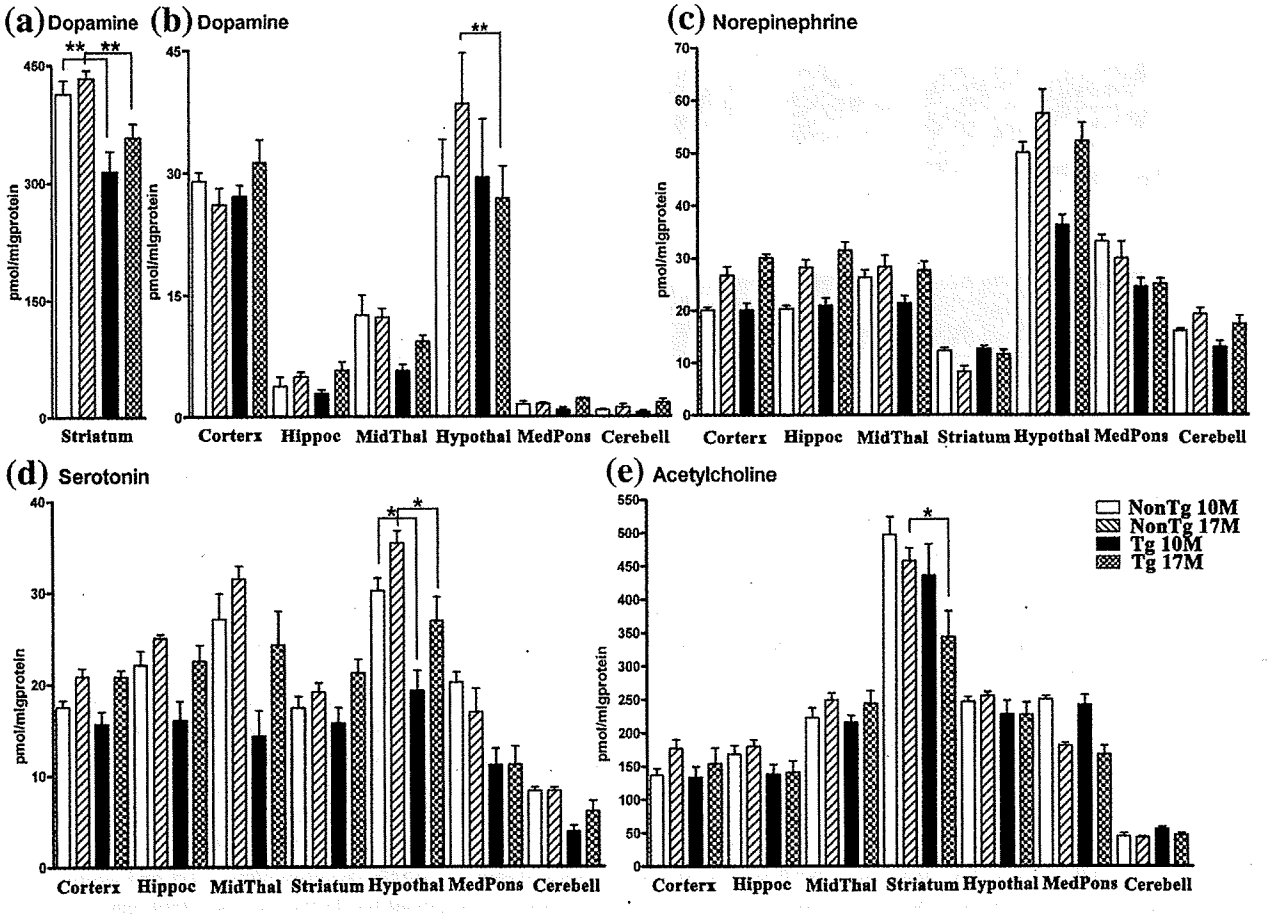

Fig. 5 – Measurement of neurochemicals. Opened column: 10-month-old non-Tg mice, Oblique column: 17-month-old non-Tg mice; Closed black colored column: 10-month-old TgαSYN mice, Crossed column: 17-month-old non-Tg mice. Cortex: cerebral cortex, Hippoc: hippocampus, MidThal: midbrain–thalamus, Hypothal: hypothalamus, MedPons: medulla–pons, Cerebell: cerebellum. *$p<0.01$, **$p<0.05$. Statistical analysis of neurochemicals between the TgαSYN and non-Tg control groups at the same age was conducted by a two-way repeated measure ANOVA (GraphPad Prism 4). (a) DA was significantly decreased in the striatum in 10- and 17-month-old TgαSYN compared with non-Tg control mice. (b) A decrease in dopamine was detected significantly in the hypothalamuses of 17-month-old TgαSYN brains ($p=0.0079$). (c) Norepinephrine (NE) was not decreased in 10- and 17-month-old TgαSYN brains. (d) Serotonin (5-HT) was decreased in the hypothalamus of 10- and 17-month-old TgαSYN brains ($p=0.0079$, $p=0.0286$, respectively). (e) ACh was decreased in the striatum of 17-month-old TgαSYN ($p=0.0286$).

The α-synuclein pathologies in TgαSYN were accompanied by decreased tyrosine hydroxylase-positive neurons, Substance P synapses and severe astrocytosis. These histological α-synuclein pathologies were also detected at the biochemical level. Accumulated αSYN was phosphorylated, ubiquitinated and sarcosyl-insoluble, suggesting that it may be conformationally changed as reported in PD/DLB brains (Hasegawa et al., 2002). The presence of higher molecule phosphorylated and ubiquitinated bands (22/29 kD) on Western blots also indicated that accumulated αSYN was modified and aggregated.

The severe decrease in DA and loss of dopaminergic neurons in SNc and the striata of PD brains is widely believed to be the pathological and biochemical cause of PD. Notably, our TgαSYN demonstrated decreased DA production in a disturbed DA system which was measured in the liquid chromatographic systems. Although other neurochemicals were altered slightly, a prominently decreased level of DA was revealed in the striatum of TgαSYN. These findings suggest selective neurotoxicity with αSYN accumulation.

In our mouse model, approximately a 20% reduction in DA in the striatum was observed when motor impairment existed. Since the rotarod test revealed significant decreased spontaneous movement, the phenotype of TgαSYN is quite similar to the cardinal clinical symptom of PD, akinesia. A decreased level of TH-positive neurons and substance P synapses also suggested that the motor impairment in TgαSYN may be caused by aberrant αSYN processes.

Our TgαSYN is a mammalian model animal showing decreased DA and motor deficits, which were certainly detected by the liquid chromatographic systems and rotarod test. For this reason, TgαSYN is a useful model for analyzing the aberrant cascade induced by pathological metabolism and aggregation of mutant αSYN, and may be useful for developing essential treatments for α-synucleinopathies such as PD and DLB.

4. Experimental procedures

4.1. *Transgene construction, generation of transgenic mice and analyses of RT-PCR*

Human αSYN A30P+A53T cDNA (450 bp) was ligated into Hind III sites in the human Thy-1 genome gene. The transgene hThy1-αSYN A30P+A53T consisted of an 8.1 kb XhoI–NcoI fragment of pBluescript II KS kidney enhancer (Fig. 1a). The CX-EGFP transgene consisted of a 3 kb Xba I/BamH I fragment of pCAGGS containing the CMV enhancer, β-actin promoter, a part of the rabbit β-globin gene, a part of the second intron, the third exon and 3′-untranslated region and cDNA of EGFP (Enhanced green fluorescent protein) with the Kozak sequence (Imai et al., 1999). Approximately 2,000 copies of the transgene with a 1:1 mole rate mixture of the hThy1-αSYN A30P+A53T and CX-EGFP as a transgene marker were micro-injected into the pronuclei of fertilized BDF1 eggs. To analyze gene expression of human αSYN, RT-PCR was performed using 2 μl of mRNA, isolated using the QuickPrep Micro mRNA purification kit (GE Healthcare Bio-Sciences Corp., Piscataway, NJ), from the brains of TgαSYN (#8713) and non-Tg mice brains at 3, 8, 17 months of age ($n=3$, respectively) in the reaction tube of Ready-To-Go RT-PCR Beads (GE Healthcare Bio-Sciences Corp., Piscataway, NJ) with PCR primer sets as follows: (αSYN forward primer: TG GAT GTA TTC ATG AAA GGA, αSYN reverse primer: CC AGT GGC TGC TGC AAT GCT C; EGFP forward primer: TGG TGA GCA AGG GCG AGG AG; EGFP reverse primer: TCG TGC TGC TTC ATG TGG TC). For semi-quantification, RT-PCR of β-actin was performed as an internal control (Elliott, 2001). Ten microliters of PCR products were analyzed by 2.5% agarose gel electrophoresis. The intensity of ethidium-stained bands was analyzed by Scion Image (Scion Corporation, Frederick, MD).

4.2. *Histological examinations*

After mice were sacrificed under anesthesia, the brains were removed and cut sagittally along the midline. One hemisphere was fixed in 0.1 mol/L phosphate buffer (PB, pH 7.6) containing 4% paraformaldehyde, and embedded in paraffin. For immunostaining, 5-μm sections were treated with 99% formic acid for 3 min, or treated in a microwave at 500 W for 5 min three times in 10 mmol/L citrate buffer (pH 6.0). After blocking with 5% normal goat or horse serum in 50 mmol/L phosphate buffered saline (PBS) containing 0.05% Tween-20 and 4% Block-Ace (Snow brand, Sapporo, Japan), sections were incubated with primary antibodies for 6 h. Specific labeling was visualized using a Vectastain Elite ABC kit (Vector, Burlingame, CA). Immunostained tissue sections were counterstained with hematoxylin. Nissl, Hematoxylin–eosin (H–E), and Gallyas–Braak stains were also done.

The following antibodies were used: mouse monoclonal antibody to human αSYN, LB509 (×4, residues 115–121/122) (Baba et al., 1998); mouse monoclonal antibody to αSYN, 42/α-Synuclein (×50, BD Transduction Laboratories, San Jose, CA); rabbit polyclonal antibody to phosphorylated Serine at residue 129 of human αSYN, PSer129 (×200) (Fujiwara et al., 2002; Hasegawa et al., 2002); rabbit polyclonal antibody to tyrosine hydroxylase (TH), AB151 (×2,000, CHEMICON, Temecula, CA); rabbit polyclonal antibody to substance P, AB1566 (×1,000, CHEMICON, Temecula, CA); rabbit polyclonal antibody to ubiquitin, UbiQ (×500) (Ikeda et al., 2005; Murakami et al., 2006); mouse monoclonal antibody to nitrated α/β SYN, Syn12 (×400, Invitrogen, Corps., Carlsbad, CA); rabbit polyclonal antibody to glial fibrillary acidic protein (GFAP, ×20,000, DAKO, Carpinteria, CA).

For electron microscopic (EM) studies, the brain tissues were immersed in a fixative solution (2.5% glutaraldehyde, 0.1 mol/L phosphate buffer (PB), pH 7.4) for 4 h and washed several times in 0.1 mol/L PB containing 7% sucrose. Blocks were then postfixed in 2% osmium tetroxide, dehydrated in ethanol and propylene oxide, and embedded in Quetol 812 (Nisshin EM, Tokyo, Japan). Ultrathin sections were stained with uranyl acetate and lead acetate prior to observation.

4.3. *Western blot analysis*

Half of each brain was homogenized in 3 ml/g of low-salt buffer (LS: 10 mmol/L Tris, 5 mmol/L ethylenediaminetetraacetic acid (EDTA), 1 mmol/L dithiothreitol (DTT), 10% sucrose, and a cocktail of protease inhibitors (Complete®, Roche Diagnostics, Indianapolis, IN), pH 7.5) and centrifuged at 25,000 g for 30 min at 4 °C (LS-soluble fraction). Pellets were treated with 3 ml/g of LS with 1% Triton X-100 and 0.5 mol/L NaCl, and centrifuged at 180,000 g for 30 min at 4 °C (Triton-soluble fraction). Pellets were then homogenized again in 2 ml/g LS with 1% N-lauroylsarcosine (SIGMA CHEMICAL CO. St Louis, MO) and 0.5 mol/L NaCl, incubated at 22 °C on a shaker for 1 h, and centrifuged at 180,000 g for 30 min at 22 °C. Supernatants were analyzed as sarcosyl-soluble fraction (Iwatsubo et al., 1996; Hasegawa et al., 2002; Sampathu et al., 2003; Ikeda et al., 2005; Murakami et al., 2006). The remaining pellets obtained from each sarcosyl-insoluble fraction were boiled at 70 °C in 20 μl of NuPAGE® LDS Sample Buffer for 10 min. Each fraction was separated on 4 to 12% NuPAGE Bis–Tris Gels (Invitrogen, Corps., Carlsbad, CA) and the blots were labeled by a mouse monoclonal antibody to human αSYN (LB509, ×4), and a mouse monoclonal antibody to phosphorylated Serine at residue 129 of human αSYN (pSyn#64, ×200, Wako, Japan). Signals were visualized with an enhanced chemiluminescence detection system (SuperSignal West® Dura Extended Duration Substrate, PIERCE, Rockford, IL) and quantified by a luminoimage analyzer (LAS 1000-mini, Fuji film, Tokyo, Japan).

4.4. *Measurement of neurochemicals*

Neurochemicals, including dopaminergic (dopamine: DA, 3,4-dihydroxyphenylacetic acid: DOPAC, homovanillic acid: HVA), noradrenergic (norepinephrine: NE, 3-methoxy-4hydroxyphenylglycol: MHPG), serotonergic (5-hydroxytryptamine: 5-HT, 5-hydroxyindoleacetic acid: 5-HIAA) and cholinergic (acetylcholine: ACh, choline: Ch) systems in the brain were measured in Tg mice ($n=10$) and non-Tg control mice ($n=10$) at 10 and 17 months old, respectively. In brief, each animal was anesthetized with Nembutal® (Dainippon Pharmaceutical Co. Ltd., pentobarbital sodium), sacrificed, and irradiated with microwaves (NJE 2603 Microwave device, New Japan Radio, Kamifukuoka, Japan) at 9.0 kW for 0.42 s to prevent post-mortem

changes in the neurochemicals during brain sampling (Ikarashi et al., 1985, 2004). The brain was removed from the skull and dissected into seven regions (cerebral cortex, hippocampus, midbrain–thalamus, striatum, hypothalamus, medulla–pons and cerebellum) according to the established method (Glowinski and Iversen, 1966), and then each region was weighed. Each dissected brain region was homogenized with 0.5 ml of 0.1 mol/L perchloric acid containing 0.8 nmol isoproterenol hydrochloride as an internal standard for the determinations of catecholamines, indoleamines and related metabolites, and 5 nmol ethylhomocholine iodide as an internal standard for the determinations of ACh and Ch, using an ultrasonic cell disrupter (US-300T, Nissei, Tokyo, Japan). The homogenate was centrifuged at 17,300 g at 4 °C for 15 min. The supernatant was filtered through a 0.45 μm millipore filter. Aliquots, typically 10 μl of the filtrates, were injected into the liquid chromatographic systems (Eicom HPLC-ECD system, Eicom Co. Ltd., Kyoto, Japan) to determine catecholamines-, indoleamines-, and acetylcholine-related substances (Ikarashi et al., 1992). The sediment was re-homogenized with 2 ml of 1 mol/L NaOH for a protein assay, which was performed using the method of Lowry et al. (1951). The concentrations of neurochemicals in the brain were expressed as the values per milligram of protein.

4.5. *Behavioral experiments*

4.5.1. *Rotarod test*

TgαSYN (n=10) and age-matched control mice (n=10) at one month to 10.5 months old were examined by the rotarod performance test according to a previous method (Kuribara et al., 1977; Ikarashi et al., 2004). Mice were placed on the rotating rod of the apparatus (Ugo basile, biological research apparatus, Milan, Italy) at a speed of 16 rpm for 300 s, and the time they stayed on the rotating rod was measured. Each set of three trials was performed at 10 minute intervals each day for every mouse.

4.6. *Statistical analyses*

Two-way repeated measures ANOVA followed by the Mann–Whitney U test for the rotarod test and open field test, and two-way ANOVA followed by Student's t test to analyze neurochemicals were performed using GraphPad Prism 4 (GraphPad Software Inc., San Diego, CA) and SPSS 10.0 (SPSS 10.0 for Windows, SPSS Inc., Chicago, IL). The means of all data are presented with their standard errors (mean ± S.E.).

Acknowledgments

We thank Dr. T Iwatsubo for coordinative provision of the LB 509 antibody and polyclonal phosphorylated αSYN antibody, Dr. D Dickson for the antibody Ubi-Q and Dr. S Kawabata for the human Thy-1 gene. We thank Dr. H Sugimoto and Dr. T Izumi for technical supports, and Dr. J Hirato for kind coordinative support. We also thank Y Nogami and H Narihiro for technical assistance. All animal experiments were performed according to guidelines established in the "Guide for the Care and Use of Laboratory Animals" (Japan).

REFERENCES

Abeliovich, A., Schmitz, Y., Farinas, I., Choi-Lundberg, D., Ho, W.H., Castillo, P.E., Shinsky, N., Verdugo, J.M., Armanini, M., Ryan, A., Hynes, M., Phillips, H., Sulzer, D., Rosenthal, A., 2000. Mice lacking α-synuclein display functional deficits in the nigrostriataL-DOPAmine system. Neuron 25, 239–252.

Arai, K., Kato, N., Kashiwado, K., Hattori, T., 2000. Pure autonomic failure in association with human α-synucleinopathy. Neurosci. Lett. 296, 171–173.

Baba, M., Nakajo, S., Tu, P.H., Tomita, T., Nakaya, K., Lee, V.M., Trojanowski, J.Q., Iwatsubo, T., 1998. Aggregation of α-synuclein in Lewy bodies of sporadic Parkinson's disease and dementia with Lewy bodies. Am. J. Pathol. 152, 879–884.

Chartier-Harlin, M.C., Kachergus, J., Roumier, C., Mouroux, V., Douay, X., Lincoln, S., Levecque, C., Larvor, L., Andrieux, J., Hulihan, M., Waucquier, N., Defebvre, L., Amouyel, P., Farrer, M., Destée, A., 2004. -Synuclein locus duplication as a cause of familial Parkinson's disease. Lancet 364, 1167–1169.

Chen, X., de Silva, H.A., Pettenati, M.J., Rao, P.N., St. George-Hyslop, P., Roses, A.D., Xia, Y., Horsburgh, K., Ueda, K., Saitoh, T., 1995. The human NACP/α-synuclein gene: chromosome assignment to 4q21.3–q22 and TaqI RFLP analysis. Genomics 26, 425–427.

Chishti, M.A., Yang, D.S., Janus, C., Phinney, A.L., Horne, P., Pearson, J., Strome, R., Zuker, N., Loukides, J., French, J., Turner, S., Lozza, G., Grilli, M., Kunicki, S., Morissette, C., Paquette, J., Gervais, F., Bergeron, C., Fraser, P.E., Carlson, G.A., George-Hyslop, P.S., Westaway, D., 2001. Early-onset amyloid deposition and cognitive deficits in transgenic mice expressing a double mutant form of amyloid precursor protein 695. J. Biol. Chem. 276, 21562–21570.

Choi, W., Zibaee, S., Goedert, M., 2004. Mutation increases phospholipids binding and assembly into filaments of human α-synuclein. FEBS Lett. 576, 363–368.

Citron, M., Eckman, C.B., Diehl, T.S., Corcoran, C., Ostaszewski, B. L., Xia, W., Levesque, G., St. George-Hyslop, P., Younkin, S.G., Selkoe, D.J., 1998. Additive effects of PS1 and APP mutations on secretion of the 42-residue amyloid β-protein. Neurobiol. Dis. 5, 107–116.

Clayton, D.F., George, J.M., 1998. The synucleins: a family of proteins involved in synaptic function, plasticity, neurodegeneration and disease. Trends. Neurosci. 21, 249–254.

Conway, K.A., Rochet, J.C., Bieganski, R.M., Lansbury Jr., P.T., 2001. Kinetic stabilization of the α-synuclein protofibril by a dopamine-α-synuclein adduct. Science 294, 1346–1349.

Elliott, J.L., 2001. Cytokine upregulation in a murine model of familial amyotrophic lateral sclerosis. Brain Res. Mol. Brain Res. 95, 172–178.

Fujiwara, H., Hasegawa, M., Dohmae, N., Kawashima, A., Masliah, E., Goldberg, M.S., Shen, J., Takio, K., Iwatsubo, T., 2002. -Synuclein is phosphorylated in synucleinopathy lesions. Nat. Cell Biol. 4, 160–164.

Galvin, J.E., Giasson, B., Hurtig, H.I., Lee, V.M., Trojanowski, J.Q., 2000. Neurodegeneration with brain iron accumulation, type 1 is characterized by α-, β-, and γ-synuclein neuropathology. Am. J. Pathol. 157, 361–368.

George, J.M., Jin, H., Woods, W.S., Clayton, D.F., 1995. Characterization of a novel protein regulated during the critical period for song learning in the zebra finch. Neuron 15, 361–372.

Giasson, B.I., Duda, J.E., Quinn, S.M., Zhang, B., Trojanowski, J.Q., Lee, V.M., 2002. Neuronal α-Synucleinopathy with severe movement disorder in mice expressing A53T human α-synuclein. Neuron 34, 521–533.

Glowinski, J., Iversen, L.L., 1966. Regional studies of catecholamines in the rat brain. I. The disposition of [^{3}H]norepinephrine, [^{3}H]dopamine and [^{3}H]dopa in various regions of the brain. J. Neurochem. 13, 655–669.

Goedert, M., 2000. -synuclein and neurodegenerative diseases. Nat. Rev. Neurosci. 2, 492–501.

Hardy, J., Gwinn-Hardy, K., 1998. Genetic classification of primary neurodegenerative disease. Science 282, 1075–1079.

Hasegawa, M., Fujiwara, H., Nonaka, T., Wakabayashi, K., Takahashi, H., Lee, V.M., Trojanowski, J.Q., Mann, D., Iwatsubo, T., 2002. Phosphorylated α-synuclein is ubiquitinated in alpha-synucleinopathy lesions. J. Biol. Chem. 277, 49071–49076.

Ikarashi, Y., Harigaya, Y., Tomidokoro, Y., Kanai, M., Ikeda, M., Matsubara, E., Kawarabayashi, T., Kuribara, H., Younkin, S.G., Maruyama, Y., Shoji, M., 2004. Decreased level of brain acetylcholine and memory disturbance in APPsw mice. Neurobiol. Aging 25, 483–490.

Ikarashi, Y., Sasahara, T., Maruyama, Y., 1985. Postmortem changes in catecholamines, indoleamines, and their metabolites in rat brain regions: prevention with 10-kW microwave irradiation. J. Neurochem. 45, 935–939.

Ikarashi, Y., Blank, C.L., Maruyama, Y., 1992. Glassy carbon pre-column for determination of acetylcholine and choline in biological samples using liquid chromatography with electrochemical detection. J. Chromatogr. 575, 29–37.

Ikeda, M., Shoji, M., Kawarai, T., Kawarabayashi, T., Matsubara, E., Murakami, T., Sasaki, A., Tomidokoro, Y., Ikarashi, Y., Kuribara, H., Ishiguro, K., Hasegawa, M., Yen, S.H., Chishti, M.A., Harigaya, Y., Abe, K., Okamoto, K., St George-Hyslop, P., Westaway, D., 2005. Accumulation of filamentous tau in the cerebral cortex of human tau R406W transgenic mice. Am. J. Pathol. 166, 521–531.

Imai, E., Akagi, Y., Isaka, Y., Ikawa, M., Takenaka, M., Hori, M., Okabe, M., 1999. Glowing podocytes in living mouse: transgenic mouse carrying a podocyte-specific promoter. Exp. Nephrol. 7, 63–66.

Iwai, A., Masliah, E., Yoshimoto, M., Ge, N., Flanagan, L., de Silva, H. A., Kittel, A., Saitoh, T., 1995. The precursor protein of non-Aβ component of Alzheimer's disease amyloid is a presynaptic protein of the central nervous system. Neuron 14, 467–475.

Iwatsubo, T., Yamaguchi, H., Fujimuro, M., Yokosawa, H., Ihara, Y., Trojanowski, J.Q., Lee, V.M., 1996. Purification and characterization of Lewy bodies from the brains of patients with diffuse Lewy body disease. Am. J. Pathol. 148, 1517–1529.

Kahle, P.J., Neumann, M., Ozmen, L., Muller, V., Jacobsen, H., Schindzielorz, A., Okochi, M., Leimer, U., van der Putten, H., Probst, A., Kremmer, E., Kretzschmar, H.A., Haass, C., 2000. Subcellular localization of wild-type and Parkinson's disease-associated mutant α-synuclein in human and transgenic mouse brain. J. Neurosci. 20, 6365–6373.

Kitada, T., Asakawa, S., Hattori, N., Matsumine, H., Yamamura, Y., Minoshima, S., Yokochi, M., Mizuno, Y., Shimizu, N., 1998. Mutations in the parkin gene cause autosomal recessive juvenile parkinsonism. Nature 392, 605–608.

Kruger, R., Kuhn, W., Muller, T., Woitalla, D., Graeber, M., Kosel, S., Przuntek, H., Epplen, J.T., Schols, L., Riess, O., 1998. Ala30Pro mutation in the gene encoding α-synuclein in Parkinson's disease. Nat. Genet. 18, 106–108.

Kuribara, H., Higuchi, Y., Tadokoro, S., 1977. Effects of central depressants on rota-rod and traction performances in mice. Jpn. J. Pharmacol. 27, 117–126.

Lee, M.K., Stirling, W., Xu, Y., Xu, X., Qui, D., Mandir, A.S., Dawson, T.M., Copeland, N.G., Jenkins, N.A., Price, D.L., 2002. Human α-synuclein-harboring familial Parkinson's disease-linked Ala-53. Thr mutation causes neurodegenerative disease with α-synuclein aggregation in transgenic mice. Proc. Natl. Acad. Sci. U. S. A. 99, 8968–8973.

Liscovitch, M., Czarny, M., Fiucci, G., Tang, X., 2000. Phospholipase D: molecular and cell biology of a novel gene family. Biochem. J. 345, 401–415.

Lotharius, J., Brundin, P., 2000. Pathogenesis of Parkinson's disease: dopamine, vesicles and α-synuclein. Nat. Rev. Neurosci. 3, 932–942.

Lowry, O.H., Rosebrough, N.J., Farr, A.L., Randall, R.J., 1951. Protein measurement with the Folin phenol reagent. J. Biol. Chem. 193, 265–275.

Masliah, E., Rockenstein, E., Veinbergs, I., Mallory, M., Hashimoto, M., Takeda, A., Sagara, Y., Sisk, A., Mucke, L., 2000. L-DOPAminergic loss and inclusion body formation in α-synuclein mice: implications for neurodegenerative disorders. Science 287, 1265–1269.

Murakami, T., Paitel, E., Kawarabayashi, T., Ikedame>M., Chishti, M.A., Janus, C., Matsubara, E., Sasaki, A., Kawarai, T., Phinney, A.L., Harigaya, Y., Horne, P., Egashira, N., Mishima, K., Hanna, A., Yang, J., Iwasaki, K., Takahashi, M., Fujiwara, M., Ishiguro, K., Bergeron, C., Carlson, G.A., Abe, K., Westaway, D., St. George-Hyslop, P., Shoji, M., 2006. Cortical neuronal and glial pathology in TgTauP301L transgenic mice: neuronal degeneration, memory disturbance, and phenotypic variation. Am. J. Pathol. 169, 1343–1352.

Neumann, M., Kahle, P.J., Giasson, B.I., Ozmen, L., Borroni, E., Spooren, W., Muller, V., Odoy, S., Fujiwara, H., Hasegawa, M., 2002. Misfolded proteinase K-resistant hyperphosphorylated α-synuclein in aged transgenic mice with locomotor deterioration and in human α-synucleinopathies. J. Clin. Invest. 110, 1429–1439.

Payton, J.E., Perrin, R.J., Woods, W.S., George, J.M., 2000. Structural determinants of PLD2 inhibition by α-synuclein. J. Mol. Biol. 337, 1001–1009.

Polymeropoulos, M.H., Lavedan, C., Leroy, E., Ide, S.E., Dehejia, A., Dutra, A., Pike, B., Root, H., Rubenstein, J., Boyer, R., Stenroos, E.S., Chandrasekharappa, S., Athanassiadou, A., Papapetropoulos, T., Johnson, W.G., Lazzarini, A.M., Duvoisin, R.C., Di Iorio, G., Golbe, L.I., Nussbaum, R.L., 1997. Mutation in the α-synuclein gene identified in families with Parkinson's disease. Science 276, 2045–2047.

Richfield, E.K., Thiruchelvam, M.J., Cory-Slechta, D.A., Wuertzer, C., Gainetdinov, R.R., Caron, M.G., Di Monte, D.A., Federoff, H.J., 2002. Behavioral and neurochemical effects of wild-type and mutated human alpha-synuclein in transgenic mice. Exp. Neurol. 175, 35–48.

Sampathu, D.M., Giasson, B.I., Pawlyk, A.C., Trojanowski, J.Q., Lee, V.M., 2003. Ubiquitination of α-synuclein is not required for formation of pathological inclusions in α-synucleinopathies. Am. J. Pathol. 163, 91–100.

Shimura, H., Schlossmacher, M.G., Hattori, N., Frosch, M.P., Trockenbacher, A., Schneider, R., Mizuno, Y., Kosik, K.S., Selkoe, D.J., 2001. Ubiquitination of a new form of α-synuclein by parkin from human brain: implications for Parkinson's disease. Science 293, 263–269.

Shoji, M., Harigaya, Y., Sasaki, A., Ueda, K., Ishiguro, K., Matsubara, E., Watanabe, M., Ikeda, M., Kanai, M., Tomidokoro, Y., Shizuka, M., Amari, M., Kosaka, K., Nakazato, Y., Okamoto, K., Hirai, S., 2000. Accumulation of NACP/α-synuclein in Lewy body disease and multiple system atrophy. J. Neurol. Neurosurg. Psychiatry 68, 605–608.

Singleton, A.B., Farrer, M., Johnson, J., Singleton, A., Hague, S., Kachergus, J., Hulihan, M., Peuralinna, T., Dutra, A., Nussbaum, R., Lincoln, S., Crawley, A., Hanson, M., Maraganore, D., Adler, C., Cookson, M.R., Muenter, M., Baptista, M., Miller, D., Blancato, J., Hardy, J., Gwinn-Hardy, K., 2002. -Synuclein locus triplication causes Parkinson's disease. Science 302, 841.

Spillantini, M.G., Schmidt, M.L., Lee, V.M., Trojanowski, J.Q., Jakes, R., Goedert, M., 1997. -synuclein in Lewy bodies. Nature 388, 839–840.

Thiruchelvam, M.J., Powers, J.M., Cory-Slechta, D.A., Richfield, E.K., 2004. Risk factors for dopaminergic neuron loss in human α-synuclein transgenic mice. Eur. J. Neurosci. 19, 845–854.

Tofaris, G.K., Reitböck, P.G., Humby, T., Lambourne, S.L., O'Connell, M., Ghetti, B., Gossage, H., Emson, P.C., Wilkinson, L.S., Goedert, M., Spillantini, M.G., 2006. Pathological changes in dopaminergic nerve cells of the substantia nigra and olfactory bulb in mice transgenic for truncated human

α-synuclein(1–120): implications for Lewy body disorders. J. Neurosci. 26, 3942–3950.

Tu, P.H., Galvin, J.E., Baba, M., Giasson, B., Tomita, T., Leight, S., Nakajo, S., Iwatsubo, T., Trojanowski, J.Q., Lee, V.M., 1998. Glial cytoplasmic inclusions in white matter oligodendrocytes of multiple system atrophy brains contain insoluble α-synuclein. Ann. Neurol. 44, 415–422.

Ueda, K., Fukushima, H., Masliah, E., Xia, Y., Iwai, A., Yoshimoto, M., Otero, D.A., Kondo, J., Ihara, Y., Saitoh, T., 1992. Molecular cloning of cDNA encoding an unrecognized component of amyloid in Alzheimer disease. Proc. Natl. Acad. Sci. U. S. A. 90, 11282–11286.

van der Putten, H., Wiederhold, K.H., Probst, A., Barbieri, S., Mistl, C., Danner, S., Kauffmann, S., Hofele, K., Spooren, W.P., Ruegg, M.A., Lin, S., Caroni, P., Sommer, B., Tolnay, M., Bilbe, G., 2000. Neuropathology in mice expressing human α-synuclein. J. Neurosci. 20, 6021–6029.

Wakamatsu, M., Ishii, A., Ukai, Y., Sakagami, J., Iwata, S., Ono, M., Matsumoto, K., Nakamura, A., Tada, N., Kobayashi, K., Iwatsubo, T., Yoshimoto, M., 2007. Accumulation of phosphorylated α-synuclein in dopaminergic neurons of transgenic mice that express human α-synuclein J. Neurosci. Res. 85, 1819–1825.

Wakamatsu, M., Ishii, A., Iwata, S., Sakagami, J., Ukai, Y., Ono, M., Kanbe, D., Muramatsu, S., Kobayashi, K., Iwatsubo, T., Yoshimoto, M., 2008. Selective loss of nigral dopamine neurons induced by overexpression of truncated human α-synuclein in mice. Neurobiol. Aging 29, 574–585.

Zarranz, J.J., Alegre, J., Gomez-Esteban, J.C., Lezcano, E., Ros, R., Ampuero, I., Vidal, L., Hoenicka, J., Rodriguez, O., Atares, B., Llorens, V., Gomez Tortosa, E., del Ser, T., Munoz, D.G., de Yebenes, J.G., 2004. The new mutation, E46K, of α-synuclein causes Parkinson and Lewy body dementia. Ann. Neurol. 55, 164–173.

Brain Pathology ISSN 1015-6305

RESEARCH ARTICLE

Transthyretin Accelerates Vascular Aβ Deposition in a Mouse Model of Alzheimer's Disease

Henny Wati[1]; Takeshi Kawarabayashi[2]; Etsuro Matsubara[3]; Ayumi Kasai[4]; Takae Hirasawa[5]; Takeo Kubota[5]; Yasuo Harigaya[6]; Mikio Shoji[2]; Shuichiro Maeda[1]

[1] Department of Biochemistry, Interdisciplinary Graduate School of Medicine and Engineering, University of Yamanashi, 1110 Shimokato, Chuo, Yamanashi 409-3898, Japan.
[2] Department of Neurology, Hirosaki University School of Medicine, 5 Zaifu, Hirosaki 036-8562, Japan.
[3] Department of Alzheimer's Disease Research, National Institute for Longevity Sciences, National Center for Geriatrics and Gerontology, 36-3 Gengo, Morioka, Obu, Aichi 474-8522, Japan.
[4] Department of Molecular Signaling, Interdisciplinary Graduate School of Medicine and Engineering, University of Yamanashi, 1110 Shimokato, Chuo, Yamanashi 409-3898, Japan.
[5] Department of Epigenetic Medicine, Interdisciplinary Graduate School of Medicine and Engineering, University of Yamanashi, 1110 Shimokato, Chuo, Yamanashi 409-3898, Japan.
[6] Neurology Service, Maebashi Red Cross Hospital, 3-21-36 Asahi, Maebashi, Tokyo 371-0014, Japan.

Keywords
Alzheimer's disease, amyloid-β, apoptosis, tau phosphorylation, Tg2576 mouse, Transthyretin.

Corresponding author:
Shuichiro Maeda, Department of Biochemistry, Interdisciplinary Graduate School of Medicine and Engineering, University of Yamanashi, 1110 Shimokato, Chuo, Yamanashi 409-3898, Japan (Email: *smaeda@yamanashi.ac.jp*)

Received 12 October 2007; revised: 10 February 2008; accepted 12 February 2008.

doi:10.1111/j.1750-3639.2008.00166.x

Abstract

Transthyretin (TTR) binds amyloid-β (Aβ) and prevents Aβ fibril formation *in vitro*. It was reported that the lack of neurodegeneration in a transgenic mouse model of Alzheimer's disease (AD) (Tg2576 mouse) was associated with increased TTR level in the hippocampus, and that chronic infusion of anti-TTR antibody into the hippocampus of Tg2576 mice led to increased local Aβ deposits, tau hyperphosphorylation and apoptosis. TTR is, therefore, speculated to prevent Aβ pathology in AD. However, a role for TTR in Aβ deposition is not yet known. To investigate the relationship between TTR and Aβ deposition, we generated a mouse line carrying a null mutation at the endogenous *TTR* locus and the human mutant amyloid precursor protein cDNA responsible for familial AD (Tg2576/$TTR^{-/-}$ mouse) by crossing Tg2576 mice with TTR-deficient mice. We asked whether Aβ deposition was accelerated in Tg2576/$TTR^{-/-}$ mice relative to the heterozygous mutant Tg2576 (Tg2576/$TTR^{+/-}$) mice. Contrary to our expectations, the degree of total and vascular Aβ burdens in the aged Tg2576/$TTR^{-/-}$ mice was significantly reduced relative to the age-matched Tg2576/$TTR^{+/-}$ mice. Our experiments present, for the first time, compelling evidence that TTR does not suppress but rather accelerates vascular Aβ deposition in the mouse model of AD.

INTRODUCTION

Insoluble amyloid-β (Aβ) peptides, the main components of brain amyloid plaques, are thought to be the causative agent of Alzheimer's disease (AD) (11). However, Aβ is normally present in a soluble form in plasma and in the cerebrospinal fluid (CSF) (39, 40), suggesting that some other factors may modulate the aggregation of Aβ fibrils. The hypothesis that transthyretin (TTR) might play some role in the pathogenesis of AD originated from the observation that TTR in the CSF binds Aβ, and prevents Aβ fibril formation *in vitro* (36, 37). It was further observed that the levels of both TTR and its oxidized forms in the CSF were lower in patients with AD compared with the age-matched controls (2, 38). The importance of TTR in inhibition of Aβ fibril formation and toxicity *in vivo* was also suggested in two model systems: transgenic *Caenorhabditis elegans* and a transgenic mouse model of AD, Tg2576. Link reported that co-expression of Aβ peptide and TTR in transgenic *C. elegans* led to a reduction in Aβ deposits (22). Tg2576 line has high level of plasma Aβ peptides (14, 18), and develops brain Aβ deposits similar to that seen in patients with AD (15, 35) and behavioral deficits (13, 53). However, it lacks neurofibrillary tangles (NFT) (27, 48, 49) and neuronal loss (15), which are unique characteristics of patients with AD (5). Stein and Johnson reported that the lack of neurodegeneration was associated with increased level of TTR in the hippocampus of Tg2576 (43). They also reported that chronic infusion of an antibody against TTR into the hippocampus of Tg2576 mice led to increased Aβ deposits, tau hyperphosphorylation, neuronal loss and apoptosis in the CA1 neuronal field (42). Carro *et al* reported that reduced Aβ burden after insulin-like growth factor I-treatment of Tg2576 was paralleled by increased brain levels of TTR (6). Giunta *et al* reported the inhibition of Aβ aggregation and toxicity and Aβ-induced apoptotic changes by TTR in cultured cells (10).